



# Durability of Ultra Silent Pavements

Laboratory and computational study

N.C. Smits



# Durability of Ultra Silent Pavements

## A laboratory and computational study

by

N.C. Smits

to obtain the degree of Master of Science  
at the Delft University of Technology,  
to be defended publicly on Monday August 29, 2016 at 16:00.

Student number:	4039688
Project duration:	June 1, 2015 – August 29, 2016
Thesis committee:	Prof. dr. ir. A. Scarpas, TU Delft
	Ir. A. Varveri, TU Delft, supervisor
	Ir. L. J. M. Houben, TU Delft
	Dr. ir. W. Broere, TU Delft
	Ing. P. The, Rijkswaterstaat

*This thesis is confidential and cannot be made public until August 29, 2021.*

An electronic version of this thesis is available at <http://repository.tudelft.nl/>.



# Abstract

Ultra-silent pavements (USP) are developed as surface layers with excellent noise reducing properties, mainly due to their high air void content. However, the open structure of USP facilitates water intrusion and makes them vulnerable to moisture damage. Past experience has shown that USP mixtures often exhibited ravelling, and poor adhesion with the underlying layer due to moisture. This study aims to quantify the effects of moisture on the strength of USP mixtures and on their adhesion to the base course. Three different mixtures were tested and their strength degradation due to moisture was evaluated through indirect tensile tests, whereas the interlaying bonding between the USP and the underlying layer was investigated using tensile adhesion tests. Both tests were performed at dry and wet conditions, on fresh and aged materials. The results showed that moisture does not necessarily decrease the strength of USP mixtures. However, the results revealed the adverse effect of moisture on interlayer bonding.

Furthermore, moisture diffusion simulations were performed using the finite element method to investigate how different values of the moisture diffusion coefficient of the binder affects the saturation of the mixture. For this, very fine meshes of each USP mixture were made using 2D images obtained by means of CT-scanner. The analysis revealed that mixture design influences the rate in which saturation takes place.

Other properties of the USP like the dynamic stiffness modulus and the cohesive strengths are determined in the laboratory to be used for structural finite element analysis. Via a moving wheel load model, the tensile stresses at the bottom of the USP layer were compared to the adhesion strengths measured in the lab.



# Preface

This thesis is written as the final exam for my Master's degree in Civil Engineering at the Technical University of Delft. For the section of Pavement Engineering, I did this research as a part of the collaboration between the Technical University of Delft and Rijkswaterstaat. During this research, I faced many problems, some of which already existed and some had not been faced before. These problems were related to both the materials being tested and to the testing equipment (even resulting in an evacuation of the faculty), but in the end a solution was found to every problem and this thesis could be finished.

Although I did my research individually, I could not have done it completely by myself. I want to start with thanking Katerina Varveri for being my daily supervisor for the past year. I enjoyed working with her and really appreciated all help, tips and advices she gave me.

Secondly, I want to thank professor Tom Scarpas for being the head of my assessment committee. He helped me a lot by asking -sometimes- simple, but critical questions on the go, on which I sometimes did not have an answer at that time. It pushed me to think about things that I did not think of at first.

I want to thank Cor Kasbergen for spending so much time on helping me with Capa-3D, the finite element software that I used. Even when I wanted to give up parts of the FEM analysis because of time limitations, it was Cor who called me at midnight to help me out.

For the laboratory work, I want to thank Marco Poot, Jan-Willem Bientjes and Michele van Aggelen. It was great to work with them in the lab and I appreciate the time they spend on explaining and adapting the testing setups and especially, repairing them when they broke down.

My next thanks go to Lambert Houben, also member of my assessment committee and the one who kept pushing me to finish my courses. This research was always more interesting to me than my final courses, but Lambert was the one who always made sure I did not forget to study for my final exams.

My final thanks go to both Wout Broere and Peter The for also being a members in my assessment committee.

*N.C. Smits  
Delft, August 2016*



# Contents

<b>List of Figures</b>	<b>ix</b>
<b>List of Tables</b>	<b>xi</b>
<b>1 Introduction</b>	<b>1</b>
<b>2 Background &amp; Literature</b>	<b>3</b>
2.1 Introduction . . . . .	3
2.2 Field tests . . . . .	3
2.3 Moisture damage and ageing . . . . .	4
2.4 Interlayer bonding . . . . .	6
2.5 Moistre Diffusion FEM Analysis . . . . .	7
2.6 Moving Load FEM Analysis . . . . .	9
2.7 Summary . . . . .	9
<b>3 Indirect tensile strength (ITS)</b>	<b>11</b>
3.1 Moisture conditioning protocol and testing procedure . . . . .	11
3.1.1 Ageing . . . . .	13
3.2 Materials . . . . .	13
3.3 Test results . . . . .	14
3.3.1 Mixture A . . . . .	14
3.3.2 Mixture B . . . . .	15
3.3.3 Mixture C . . . . .	16
3.3.4 Comparison . . . . .	20
3.4 Conclusion . . . . .	21
<b>4 Dynamic stiffness</b>	<b>23</b>
4.1 Introduction and formulae . . . . .	23
4.2 Test setup and sample preparation . . . . .	24
4.3 Results . . . . .	25
4.4 Conclusion . . . . .	30
<b>5 Interlayer bonding, using the Tensile Adhesion Test (TAT)</b>	<b>31</b>
5.1 Introduction . . . . .	31
5.2 Testing procedure and apparatus . . . . .	31
5.3 Results . . . . .	32
5.4 Conclusion . . . . .	34
<b>6 Cohesive strength</b>	<b>35</b>
6.1 Introduction . . . . .	35
6.2 Test setup and specimen preparation . . . . .	35
6.3 Results . . . . .	36
6.4 Conclusion . . . . .	37
<b>7 Finite Element Analysis: Moisture diffusion</b>	<b>39</b>
7.1 Introduction . . . . .	39
7.2 Creating the mesh . . . . .	39
7.3 FEM input . . . . .	42
7.4 Results . . . . .	43
7.4.1 Mixture A . . . . .	43
7.4.2 Mixture B . . . . .	44
7.4.3 Mixture C . . . . .	44
7.5 Conclusion . . . . .	45

---

<b>8</b>	<b>Finite Element Analysis: Moving wheel-load</b>	<b>47</b>
8.1	Introduction . . . . .	47
8.2	Mesh generation . . . . .	47
8.3	Load. . . . .	48
8.4	Results . . . . .	48
8.5	Conclusion . . . . .	52
<b>9</b>	<b>Conclusion and Recommendations</b>	<b>53</b>
9.1	Conclusion . . . . .	53
9.2	Recommendations for further research . . . . .	54
	<b>Bibliography</b>	<b>55</b>

# List of Figures

2.1	Test area in Stockholm	4
2.2	Application of PERS on the A50 near service area De Brink using the Rollpave technique	5
2.3	Water pumping action (pore pressure development)	5
2.4	Hardening due to ageing of a DGE/DDS epoxy system	6
2.5	Shear strengths of the interfaces and the effect of moisture conditioning	7
2.6	(a) Output locations for normalized moisture concentration and (b) air void phase of the AC specimen	8
2.7	Normalized moisture concentration profile along the diameter of the specimen at different time intervals	8
2.8	Effects of a varying elastic component in the PERS layers on the strains in the PERS	9
2.9	Dutch pavement system with USP as a top layer	9
3.1	Moisture induced Sensitivity Tester	12
3.2	Sample in ITT frame after testing	12
3.3	From left to right: Material A, B and C	13
3.4	Typical ITT output graphs for mixtures A and B	14
3.5	ITS for fresh cores of Mixture A after conditioning and MIST	15
3.6	ITS for aged cores of Mixture A after conditioning and MIST	15
3.7	ITS for fresh cores of Mixture B after conditioning and MIST	16
3.8	ITS for aged cores of Mixture B after conditioning and MIST	16
3.10	Strain rate calculations for ITT and DTT	17
3.9	Beam sawn from 100mm core	17
3.11	Uncorrected DTS for fresh cores of Mixture A after conditioning and MIST	18
3.12	Uncorrected DTS for aged cores of Mixture A after conditioning and MIST	19
3.13	Mastercurve as made by Pramesti, but recalculated for 20°C	19
3.14	Calculated ITS for fresh cores of Mixture C after conditioning and MIST	20
3.15	Calculated ITS for aged cores of Mixture C after conditioning and MIST	20
4.1	Explanation of the phase angle $\Phi$	24
4.2	Stiffness testing cabinet (L) and sample closeup (R)	25
4.3	Fourier analysis performed on the raw output data of Mixture A, beam 1 at 15 °C	26
4.4	Mastercurves for mixtures A, B and C.	27
5.1	The 3 mixtures after coring the 50mm cores.	31
5.2	Cores in the conditioning bath. Note that two cores of Mixture B are orientated in a different direction. This is because the raster of cores was what kept the cores upright. Since those 2 were not in the raster, they were placed flat so that they would not wobble around by the currents in the bath.	32
5.3	Specimen in the testing setup	33
5.4	Failed TAT cores for mixtures A, B and C	33
5.5	Tensile adhesion strength after moisture conditioning	34
6.1	Test setup for determination of cohesive strength	35
6.2	Typical behaviour for each mixture at 20°C and a displacement of 23.8mm/min. Note the different span of the x-axis for mixture C.	36
7.1	Cubic element after CT scanning showing (a) the rubber (yellow) and binder (blue), (b) the aggregates and (c) the air voids of the material.	39
7.2	CT scan of Mixture C	40

---

7.3	A slice of the beam shown in figure 7.2	40
7.4	Coloured based on greyscale	41
7.5	Coloured 3D cube of mixture C	41
7.6	Only the aggregates of mixture C	42
7.7	Final mesh	42
7.8	FE Results for Mixture A	43
7.9	FE Results for Mixture B	44
7.10	FE Results for Mixture C	44
8.1	Road structure as used in the preliminary research	47
8.2	Enhanced displacement under the load and stresses ( $\sigma_{xx}$ ) for Mixture A (top) and Mixture C (bottom)	49
8.3	Enhanced displacement under the load and stresses ( $\sigma_{yy}$ ) for Mixture A (top) and Mixture C (bottom)	50
8.4	Enhanced displacement under the load and shear forces ( $\tau_{xy}$ ) for Mixture A (top) and Mixture C (bottom)	51

# List of Tables

3.1	Test schedule with amount of cores to be tested . . . . .	11
3.2	TSR (%) for fresh mixtures . . . . .	21
3.3	TSR (%) for aged mixtures . . . . .	21
4.1	Phase angles . . . . .	28
4.2	Dynamic modulus values . . . . .	29
5.1	Pull-off strengths in N/mm <sup>2</sup> , averages of 3 tests . . . . .	34
6.1	Cohesive strengths in N/mm <sup>2</sup> , averages of 3 tests . . . . .	37



# Introduction

For decades, governments, road authorities, contractors and many different parties all over the world are trying to find a solution to one of the great problems that come with the great increase of traffic: noise. Noise pollution is a great social problem. Noise pollution can cause sleep disturbances, an increase in blood pressure, stress and can lead to heart diseases. The World Health Organisation (WHO) sets 55 dB as the threshold of community noise and beyond this threshold, health problems as a result of the noise become possible.

This was also investigated by the London School of Hygiene & Tropical Medicine, who analysed data for 8.6 million people in London. This research showed that there were 4% more deaths among people who lived in areas with daytime road traffic noise of more than 60dB, compared to areas where the daytime traffic noise was below 55dB. In the areas with more than 60dB traffic noise, the likeliness to be admitted in a hospital grew with 5% for adults and even 9% for elderly people (75 and older) [1].

In The Netherlands, a lot of research has been done on silent roads as well. Thin, noise reducing surface layers, single layer porous asphalt (ZOAB), double layer porous asphalt and many other solutions have been applied in the past, one more effective than the other. This research continues the path that the Dutch government has taken in order to reduce the traffic noise in The Netherlands. Based on previous researches and results, the Dutch workgroup Innovatie Programma Geluid (IPG) was formed to investigate the application of new types of ultra silent pavements (USP) and gain a traffic noise reduction of 10dB in comparison to the classical Dense Asphalt (DAC). These ultra silent pavements were developed by companies who were free to experiment with various methods. This could be the addition of elastic material like rubber, an increase in the number of air voids or other ideas they had in order to reach this traffic noise reduction.

As a part of this investigation, this research focusses on the mechanical properties of three new types of ultra silent pavements -provided by three different manufacturers- and the influence of moisture conditioning and ageing on these properties.

## Outline

Chapter 1 is this introduction and gives the outline of the report.

Chapter 2 focusses on literature. In the past, a lot of research was done on Ultra Silent Pavements and traffic noise. In this chapter, previous researches are discussed in relation to their results. To not make the same mistakes, the causes of the failures were taken into account in this new research. Another reason to look at the past researches was to see if any failures between various tests were similar. If the same failure type occurred in various tests, extra attention to this type of failure was given during this research.

Chapter 3 describes the moisture conditioning protocol that was used for conditioning the three different USP samples that were investigated. By performing this method, the effects of moisture on the strength of a material were determined via the Indirect Tensile Test (ITT). For this method, both fresh and aged samples were used to investigate if ageing had any influence on the susceptibility of the mixtures to moisture damage. Based on the results, the Indirect Tensile Strength Ratio (ITSR) was

determined and used to grade the various mixture designs. This procedure was done on both fresh and aged mixture to investigate the effects of hardening of the binder over time.

In Chapter 4, the dynamic stiffness of the various mixtures was determined. Since the materials are all viscous-elastic and therefore depend on temperature and loading frequencies, the dynamic stiffness modulus had to be determined. Via the master curve, a comparison of the stiffness of the various materials was made. The results were used as an input for finite element analysis.

In Chapter 5 the adhesion between two layers was tested. From the literature was found that in quite some cases, the bond between an underlying porous asphalt (PA) layer and an USP weakened due to moisture conditioning. Therefore, the same conditioning protocol as in Chapter 2 was applied, but instead of an ITT, a pull-off test was done. The strengths were measured after various conditioning periods and the decrease in strength is presented in a ratio with the dry strength.

Chapter 6 focusses on the cohesive strength of the three mixtures. This mechanical property gives more insight in the material behaviour and these properties can also be used in future finite element analysis's. The cohesive test was performed at two different temperatures and two different strain rates, but only on fresh material and not conditioned.

In Chapter 7, the focus shifts from laboratory research to finite element modelling. By the use of a CT-scanner, a 3D mesh of all three mixtures was made and by varying the Moisture Diffusion coefficient for the binders, the effect of this moisture diffusion coefficient on the saturation of the various mixtures was investigated. Based on the results, an explanation for the materials' susceptibility to moisture damage was tried to be found.

Chapter 8 focusses on finite element modelling too, but on a much larger scale. This time, the effect of a moving wheel-load on a road was investigated. The input parameters for the top layer were taken from the results that we found in Chapter 4 and by looking at the occurring tensile stresses at the bottom of the top layer, information about the needed tensile adhesion strength between the ultra silent pavement and the underlying porous asphalt was gained.

Chapter 9 contains a discussion about all outcomes and results, and ends with a conclusion and future recommendations.

# 2

## Background & Literature

### 2.1. Introduction

Since the 1970's, research is done on ultra-silent road surfaces, which resulted in the use of poroelastic materials in road surfaces. This idea was patented by Mr Nils-Åke Nilsson, working for IFM Akustik-byrå AB in Stockholm [2]. The idea of using such materials in road surfaces was the reduction of traffic noise. Already in the 1980's, a noise reduction of already 10dB(A) was achieved [3], showing the possibilities of PERS.

In [4], the definition of a Poroelastic Road Surface (PERS) is stated as:

*A poroelastic road surface (PERS) is a wearing course for roads with a very high content of inter-connecting voids so as to facilitate the passage of air and water through it, while at the same time the surface is elastic due to the use of rubber (or other elastic products) as a main aggregate. The design air void content is at least 20% by volume and the design rubber content is at least 20% by weight.*

Therefore, PERS is by definition an asphalt pavement layer which contains rubber or any similar elastic material and still has a great amount of air voids. Although a mixture with a high percentage of air voids normally means that the mixture exists of a stone skeleton, replacing some of these aggregates with rubber particles will result in a pavement that is able to deform. When the pavement deforms under the loading of a tire, this means that the tire alone is no longer required to take all the deformation. This will result in a lower angle of attack of the tire and a reduction of traffic noise [2].

However, not just the addition of poro-elastic materials reduces the traffic noise, also the increase of air voids has a positive influence on the reduction of noise. Liu [5] showed that for a Single Layer Porous Asphalt (SLPA) and a Two Layer Porous Asphalt (TLPA), the noise reduction increases linear with the air void percentage. Both SLPA and TLPA that are applied these days in the Netherland, have an average air void content of about 20%.

### 2.2. Field tests

Since the invention of PERS, many different tests found place. In 2004, a test site with three different types was created in Stockholm. [6] Here, special attention was given to the adhesion with underlying layers. Two of the three tested mixtures (Tokai, Rosehill) consisted of prefabricated panels of 1x1m<sup>2</sup>, glued to an existing base course. The third material (Spentab) was created in situ in a classical way, using an asphalt paving machine. In the end, the Spentab material was the one that showed some spots with pore adhesion to the base layer. The test, however, had to be interrupted after a few months because of a bad adhesion between the underlying base layer and the layers below that.

After this test in Stockholm, more research on the performance of PERS as a low noise pavement was done [7]. This research in Japan focused mainly on in-situ created PERS pavements and investigated the reduction of skid resistance due to the loss of material at the surface, and the adhesion to the base layers. The reduction in skid resistance was solved by modifying the mixture, but the adhesion to the base layer remained poor. The researchers stated that the main reason for this bad adhesion was

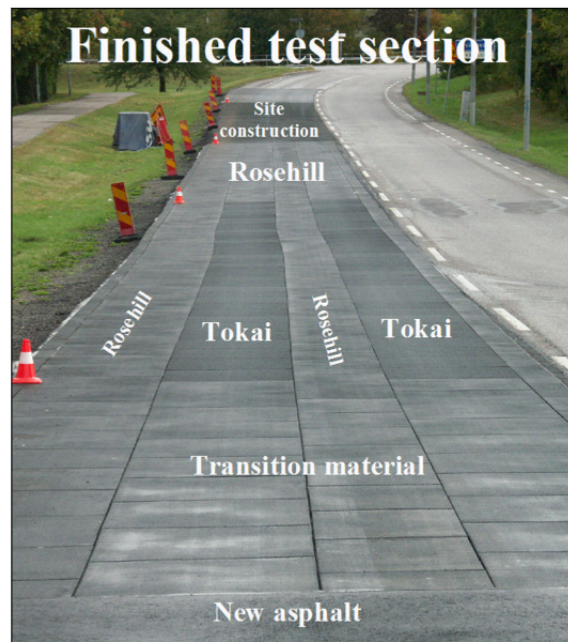


Figure 2.1: Test area in Stockholm [6]

the deformation of the base layer.

These two investigations show the importance of research in the bond between the PERS and the underlying base layers. The experiment in Stockholm also showed that before applying PERS on an existing road surface, this existing layer must have a good adhesion with the asphalt below.

Looking at the developments made on PERS in Japan, [8] states that the most effective way of applying PERS to reach the highest bond with the underlying layers, is by the use of the prefabricated panels. This showed good results on field tests in Japan, but looking at the field test in Stockholm, it gave the best results for the tests on Tokai and Rosehill as well [6].

In addition to this, Rijkswaterstaat in The Netherlands tested a PERS on a service area of the Dutch A50 as part of the "noise innovation program" program (IPG) [9]. This PERS was prefabricated in a large hall, rolled on a large drum and later, at the construction site, rolled out using the Rollpave technique. By using this technique, the PERS could be created under controlled conditions without any weather influences. Unfortunately, the initial skid resistance of the PERS was too low because the PERS kept the rainwater instead of draining it. For this reason, the test section remained closed for traffic during autumn and winter, until the skid resistance improved. This happened in the spring of the next year. By then, the mechanical properties of PERS were already highly affected by the protracted exposure to water. This caused decomposition of the PERS and the test had to be stopped after a few weeks.

### 2.3. Moisture damage and ageing

The test on the Dutch A50 showed a great decrease in strength after being immersed with water for a few months. Because of this, more research has to be done on the susceptibility of PERS to moisture. The PERS applied on a dense graded asphalt layer showed a greater decrease in strength than the PERS applied on the PA layer, probably because the standing water could drain through the PA, while it could not through the dense asphalt layer.

Since PERS is an open graded asphalt mixture, water penetrates easily in the entire layer of asphalt. This results in the exposure of a great surface to the water. When water can permeate into the bitumen and the aggregate and as a result, both the cohesive strength of the bitumen and the adhesive strength between the bitumen and the aggregate may decrease, resulting in the loss of aggregates. This is called



Figure 2.2: Application of PERS on the A50 near service area De Brink using the Rollpave technique [10]

stripping [11].

Stripping is not the only problem caused by moisture. Since moisture is incompressible, *water pumping* is another occurring problem. When water gets enclosed in the pavement due to its permeability, and the pavement is compressed under a wheel load, the water exerts a multidirectional force on all surrounding material (Figure 2.3) [12].

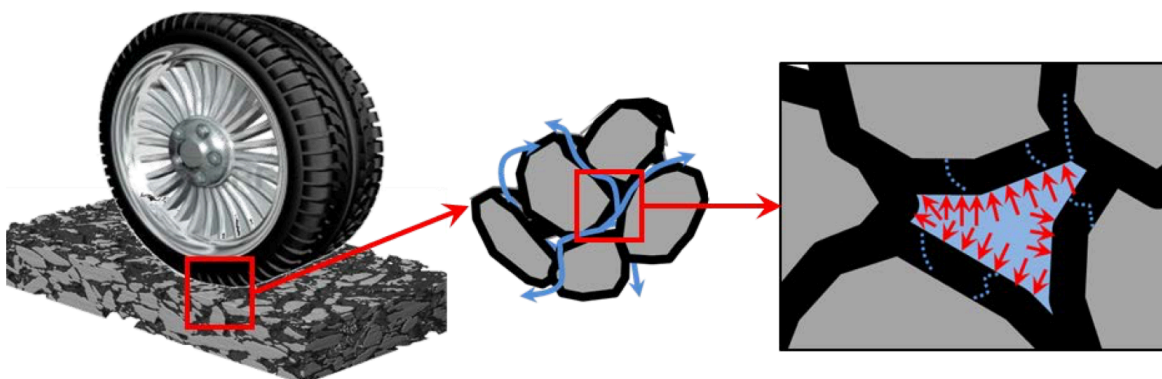


Figure 2.3: Water pumping action (pore pressure development) [12]

Both the effects of asphalt being submerged in water and asphalt being exposed to pore pressures, were investigated in a recent research by Varveri. [13] This research on porous asphalt specimens showed the effects of pure moisture conditioning and the combination of moisture conditioning in combination with cyclic pore pressures, applied by the moisture induced sensitivity tester (MIST). The effects of pure moisture conditioning on the strength of the material, can be assigned to the physical process *moisture diffusion*. Moisture diffusion is a molecular process, where water molecules can diffuse in the pores of the bitumen. The rate in which this process occurs (flux) depends on the concentration gradient of water, the temperature and the diffusion coefficient ( $D$ ) of the components of the asphalt. [14] It is assumed that for asphalt, the diffusion of moisture will follow Fick's second law of diffusion:

$$\frac{\partial \theta}{\partial t} = \nabla(D\nabla\theta)$$

Where  $0 \leq \theta \leq 1$  is the normalised moisture concentration in the material at any given time and  $D$  is the moisture diffusion coefficient. The normalised moisture concentration can be written as the the concentration at any moment in time, divided by the maximum moisture concentration:

$$\theta = \frac{C_t}{C_{max}}$$

Varveri investigated the moisture diffusion of stonemastic- and porous asphalt (SMA and PA) and used this data to set up the moisture conditioning protocol which will - later on - be used in this research.

Regarding to ageing, a lot of research has been done on the ageing of bituminous materials, but what is more of interest for this research, is the effect of ageing on polyurethane (PU) and epoxy resin. The mixtures provided in this research all used epoxy resins as main binder.

A research by Hollingsworth back in 1967 already showed that PU rubbers are susceptible to ageing, although the normal, dry conditioned specimens deteriorated less than the specimens who where aged and conditioned in water. [15] Odegard and Bandyopadhyay [16] show, based on gathered data from Chang and Brittain [17] how epoxy system hardens during ageing. The effect of hardening on this epoxy is shown in figure 2.4.

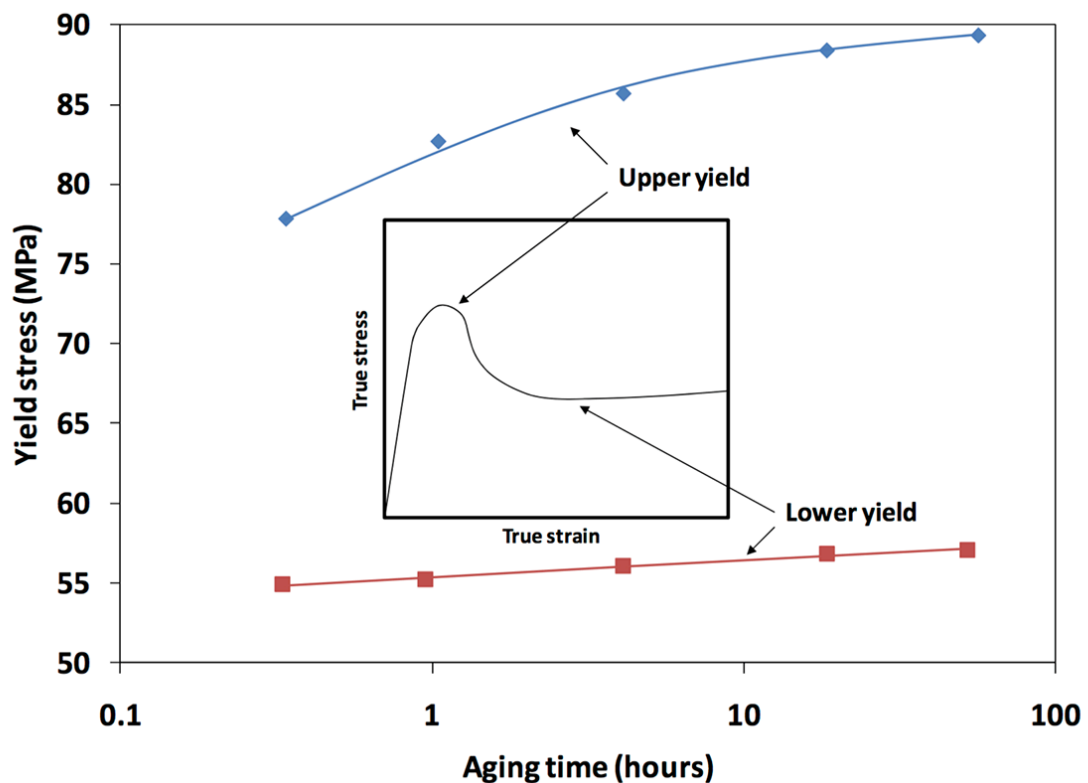


Figure 2.4: Hardening due to ageing of a DGE/DDS epoxy system [16] [17]

## 2.4. Interlayer bonding

From the field tests was seen that the interlayer bonding between the PERS and the underlying layers is an important source of failure of the road. In 2004, Raab et. al. [18] investigated the interlayer properties between asphalt layers and the influence of moisture on these properties. This research focusses on both the pull-off strength and the shear strength between two asphalt layers, but only for the shear strength, the effect of moisture was investigated.

In this research, it is shown that in shear scenarios, the bond between two asphalt layers decreased after conditioning. The tests were done on cores that were taken from a road that existed for 20 years, so they were not fresh. Still, after conditioning, the strength decreased as shown in the table in figure 2.5.

Test #	Specimen #	Pressure [bar]	Storage Time in Water at 40°C [hrs]	Shear Force [kN]	Shear Stress [N/mm <sup>2</sup> ]
1	53	0	0	25.15	1.42
1	64	0	0	29.21	1.65
1	52	0	0	26.37	1.49
2	51	0.5	5.5	22.19	1.26
2	59	0.5	5.5	22.76	1.29
2	26	0.5	5.5	24.15	1.37
2	27	0.5	5.5	21.53	1.22
3	43	0.55	8	19.05	1.08
3	48	0.55	8	21.2	1.20
3	49	0.55	8	22.14	1.25
3	4	0.55	8	19.51	1.10
4	36	0.5	8	20.39	1.15
4	5	0.5	8	19.15	1.08
4	1	0.5	8	19.08	1.08
4	6	0.5	8	21.05	1.19
5	42	0	75	14.54	0.82
5	41	0	75	18.95	1.07
5	34	0	75	23.98	1.36
5	45	0	75	21.25	1.20
5	2	0	75	19.21	1.09

Figure 2.5: Shear strengths of the interfaces and the effect of moisture conditioning [18]

## 2.5. Moistre Diffusion FEM Analysis

The effect of moisture on the mechanical properties of the mixtures is up to some extent related to the rate in which moisture can penetrate into the mixture. Not only because of the percentage of air voids, but also because of the diffusion of water into the mastic, the rubber and the aggregates. To have an idea of the rate in which this diffusion occurs, a finite element model was used. Each mixture was scanned using a CT scanner and these scans were transformed into a finite element mesh.

This same method was performed by, and described in the earlier mentioned research by Varveri [12]. By making a mesh from a CT-scanned piece of asphalt, the rate of saturation of certain nodes can be calculated by using finite element software. In the case of Varveri, circular samples were used, as shown in figure 2.6.

With this mesh, Varveri showed how the moisture concentration varied over the specimen and over time. This is shown in figure 2.7.

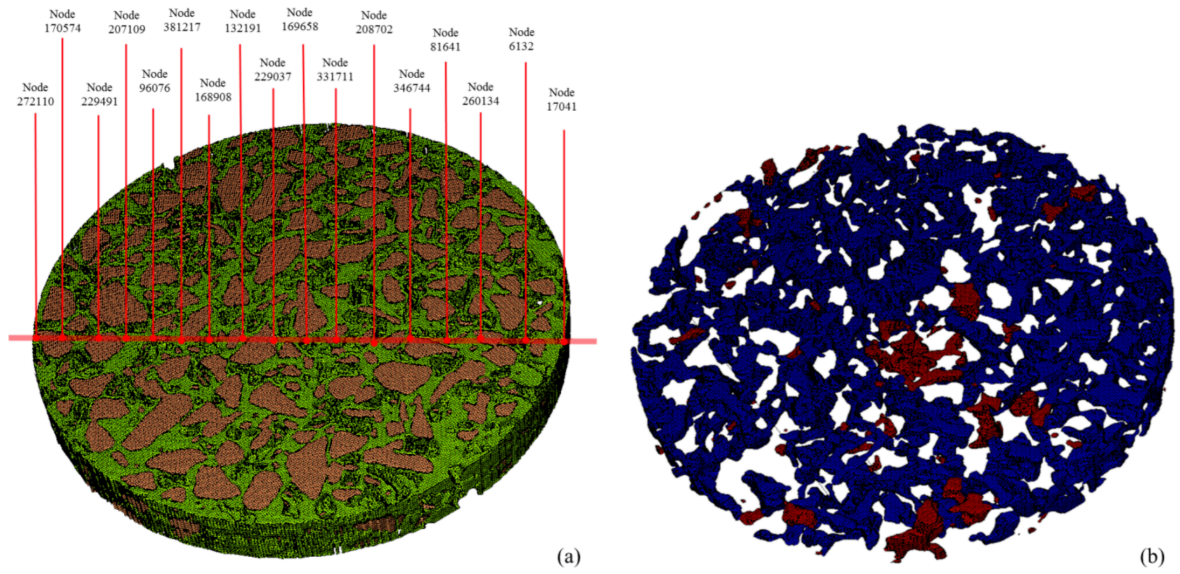


Figure 2.6: (a) Output locations for normalized moisture concentration and (b) air void phase of the AC specimen [12]

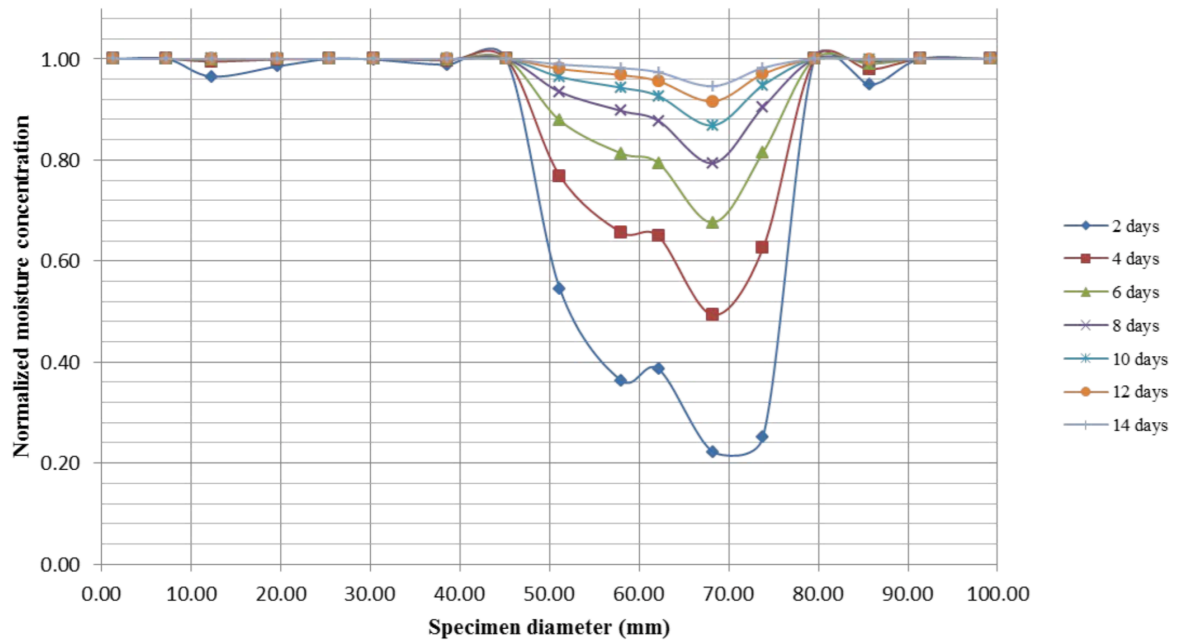


Figure 2.7: Normalized moisture concentration profile along the diameter of the specimen at different time intervals [12]

## 2.6. Moving Load FEM Analysis

In the preliminary phase of this project, a moving load model was used to get information on the required strengths and stiffnesses of each mixture in relation to the strengths and stiffnesses of the surface layer [19]. By use of this computational analysis, suppliers of USP for this master thesis received information about stiffnesses and advisable material stiffness properties. This FE analysis showed how a decrease in stiffness increased the strains in the PERS layer, as showed in figure 2.8.

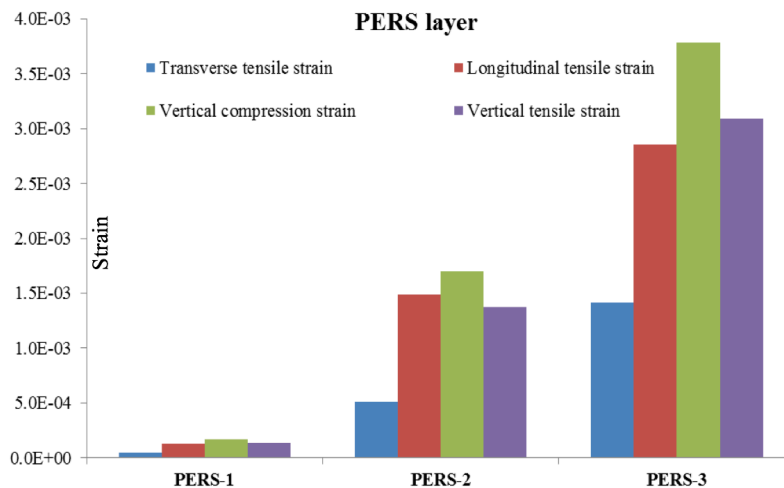


Figure 2.8: Effects of a varying elastic component in the PERS layers on the strains in the PERS [19]

In figure 2.8, the varying elastic components ( $E$ ) for the 3 different PERS mixtures were taken as  $1.3 \cdot 10^{07} \text{ N/m}^2$  (PERS-1),  $1.3 \cdot 10^{05} \text{ N/m}^2$  (PERS-2) and  $1.3 \cdot 10^{04} \text{ N/m}^2$  (PERS-3).

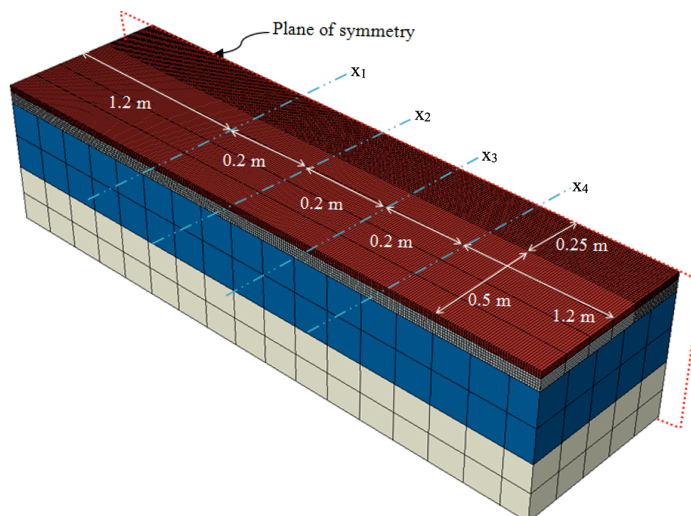


Figure 2.9: Dutch pavement system with USP as a top layer [19]

## 2.7. Summary

Based on these previous researches on the effects of moisture conditioning and ageing on PERS, epoxy and PU materials, the results of field tests and the wish for a higher reduction of traffic noise, enough support can be found to perform more specific tests on new mixture designs before performing a new field test. The goal will be to determine the mechanical properties of Ultra Silent Pavement mixtures and the effect of moisture conditioning and ageing on these mechanical properties. This properties will be determined in a controlled, laboratory environment, in order to be able to repeatedly perform a test

under the same conditions. By doing this, fair comparisons can be made between various mixtures with complete different properties in order to select the mixture for a field test. The results gathered from laboratory tests can thereafter be used in finite element calculations.

# 3

## Indirect tensile strength (ITS)

### 3.1. Moisture conditioning protocol and testing procedure

The goal of the test was to determine the degradation of the Indirect Tensile Strength (ITS) of the specimens, due to the exposure to water (conditioning) and cyclic pore pressures as described by Varveri [?]. Each material was conditioned for two and four weeks, and after each period of conditioning, on half of the specimens cyclic pore pressure was applied using the Moisture Induced Sensitivity Test (MIST).

The MIST (figure 3.1) is a device that has an enclosed tank which can contain three specimens of asphalt. After placing the specimens, the tank was filled with water before closing it. The final bit of air was replaced with water via an external valve, so that no air remained in the bucket. Any air would not allow the device to increase the pressure to the required value. The water was heated to 60°C and via an expanding bladder, the MIST is able to raise and release the pressure in the tank for 4000 times, up to a pressure of 75 psi (=0.52 MPa).

For each mixture, 24 cores were available to determine the effects of conditioning and cyclic pore pressure on the ITS. Those 24 cores were divided into two sets of 12. Set one was kept dry to determine the effect of MIST on unconditioned samples (three cores) and to have a reference ITS for dry and unconditioned material every two weeks (nine cores). The other set was used for conditioning: six cores two weeks and the other six cores four weeks. Table 3.1 gives an overview of this.

	0 weeks	2 weeks	4 weeks
Conditioned	-	3 ITT	3 ITT
	-	3 MIST + ITT	3 MIST + ITT
Unconditioned	3 ITT	3 ITT	3 ITT
	3 MIST + ITT	-	-

Table 3.1: Test schedule with amount of cores to be tested

When the cores were not being conditioned or in the MIST, they were stored in a climate chamber at 15°C.

The Indirect Tensile Test (ITT) was performed according to the Dutch standards [20], at:

- 20°C - Test temperature
- $50.8\text{mm} \times \text{s}^{-1}$  - Vertical deformation speed (Marshall speed)

The night before testing, the specimens were already placed in a climate cabinet at 20°C.

The ITT testing frame existed of two strips with a width of 12.7mm and an inner diameter of 101.6mm. This setup is shown in figure 3.2.



Figure 3.1: Moisture induced Sensitivity Tester

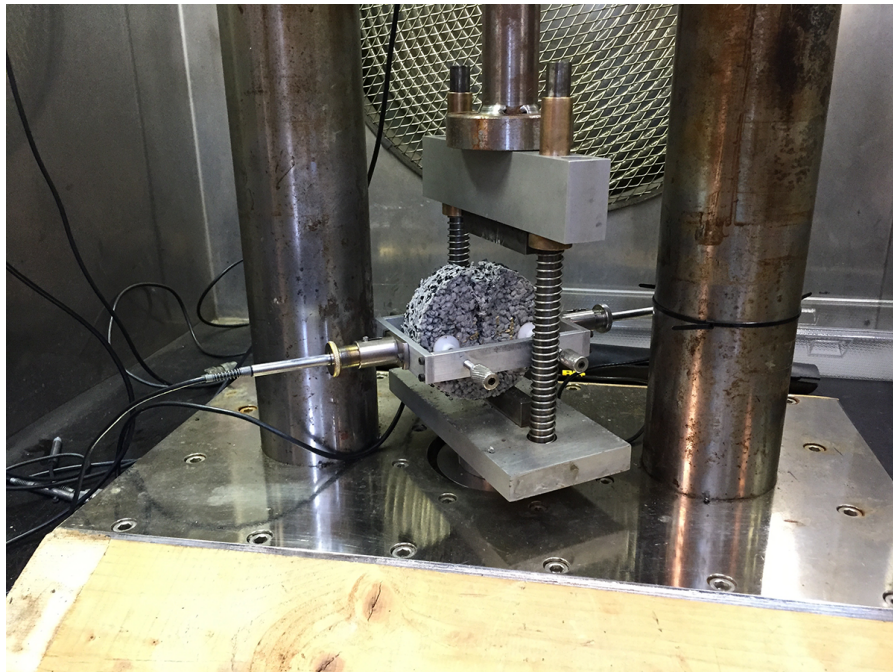


Figure 3.2: Sample in ITT frame after testing

### 3.1.1. Ageing

To see the effects of ageing on the indirect tensile strength, the entire procedure as described, was done on two subsets of 24 cores per mixture. One subset was tested as is, while the second subset was aged first. This was done by storing them in an oven at 60°C for a period of four weeks. In total, for the three mixtures together, 144 cores were tested.

## 3.2. Materials

The materials described in this research were all three very different from each other and only two could be called PERS, since one material did not contain any rubber. At first sight, one can see the differences between the mixtures. Figure 3.3 shows a beam of every material.

- **Mixture A** - This one looked like a fine graded mixture, composed from sharp-edged particles and a large amount of air voids. It felt very stiff and it did not contain any elastic materials or bitumen.
- **Mixture B** - The color drew the attention. It looked almost white, which indicates the use of resin instead of bitumen. It looked less open graded than mixture A, although it was definitely not dense. The mixture was build up with fine graded and sharp edged aggregates and rubber particles. Despite the use of resin, the addition of rubber made it feel like a flexible material.
- **Mixture C** - The most remarkable of this mixture was the lack of sharp edge particles. It existed of small, round balls instead of aggregates. Further investigation showed that these balls existed of aggregates, enrobed with rubber. Although the material was black and it looks like bitumen was used, the remains of resin proofed the opposite. At last, the mixture felt very elastic, which was not a surprise when looking at the amount of rubber.

It would have been very useful if more details about the exact composition of the various USP were available, but since they are all commercial products, this information was not shared and therefore no details on this can be shared in this report.



Figure 3.3: From left to right: Material A, B and C

### 3.3. Test results

Mixture A did not give any problems during the ITT. This mixture usually resulted in nice and steep graphs, indicating an immediate split of the material. Mixture B showed a more ductile behaviour, resulting in a more flattened graph in comparison to mixture A. A typical graph for both Mixture A and Mixture B is shown in figure 3.4.

Mixture C turned out to be so elastic that the Indirect Tensile Strength could not be determined. In order to make a valid comparison between the three different mixtures, we decided to determine the Direct Tensile Strength for mixture C. More on this in chapter 3.3.3.

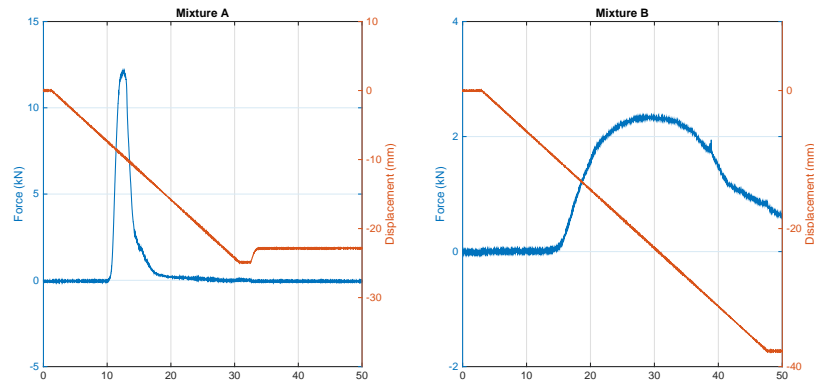


Figure 3.4: Typical ITT output graphs for mixtures A and B

#### 3.3.1. Mixture A

For the fresh cores of mixture A, both the dry ITS and the conditioned ITS were relatively constant over the various time intervals. For the fresh conditioned specimens on which also the MIST was done, the ITS did decrease. The results are shown in figure 3.5. The error bars show the difference between the highest and the lowest test result. The effect of the cyclic pore pressure on the strength of the material can be attributed mainly to the high stiffness of the mixture A, due to the use of only aggregates and binder and the absence of rubber particles. This did not allow the redistribution of the internal pressure induced stresses, and therefore lead to damage of the material.

For the aged cores of mixture A, the graph looks a bit more unexpected. Due to ageing, the binder was expected to become harder, resulting in an increase in dry ITS. This is only very little the case and even still within the error range, so no conclusions can be made on this. The strength after two weeks decreased expectedly, but after four weeks increased back to almost the original strength. Some extra tests were done to exclude any problems with the test setup, but since all cores were cored from slabs, it might be the case that the cores for week two had a different composition. The results are shown in figure 3.6.

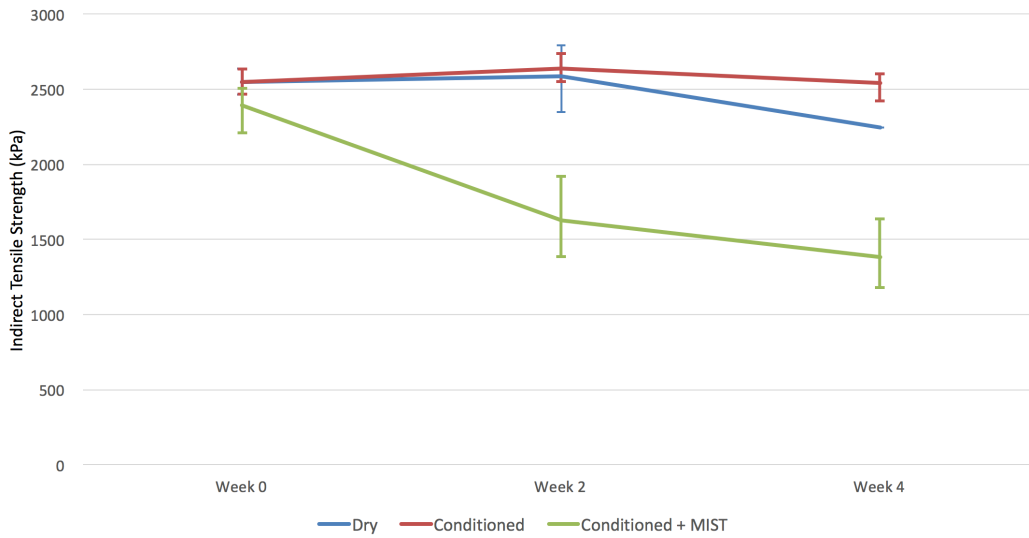


Figure 3.5: ITS for fresh cores of Mixture A after conditioning and MIST

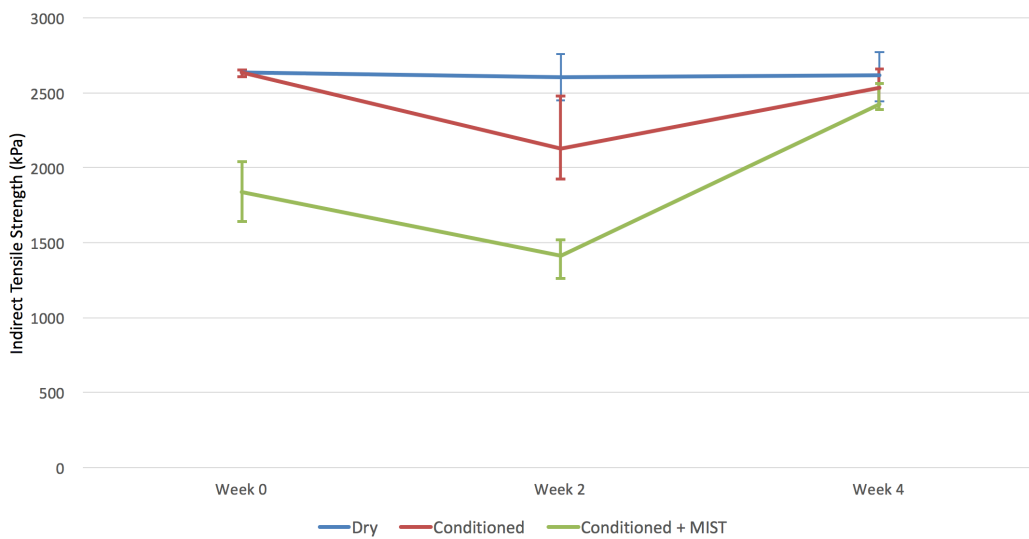


Figure 3.6: ITS for aged cores of Mixture A after conditioning and MIST

### 3.3.2. Mixture B

Mixture B behaved very different than mixture A. Already within the four weeks of the conditioning protocol, the unconditioned samples hardened. This made the material look susceptible to ageing. The same thing happened to the cores that were aged for four weeks in an oven. Here, the initial ITS was much higher too. However, this does not automatically mean that the material stiffened due to the ageing in the oven: Since the hardening of the material goes relatively fast, it might be that the cores that were used for the aged tests, were older than the cores used for the fresh test.

For both the fresh and the aged tests, it was clear that the ITS decreased a lot after conditioning and the effect of MIST was not very high. The material has enough capacity to deform under the cyclic pore pressure.

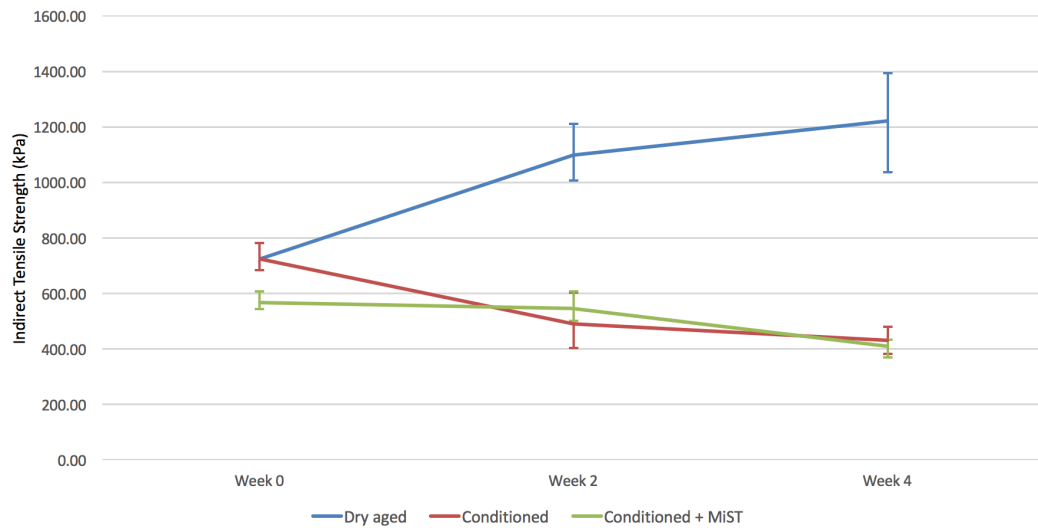


Figure 3.7: ITS for fresh cores of Mixture B after conditioning and MIST

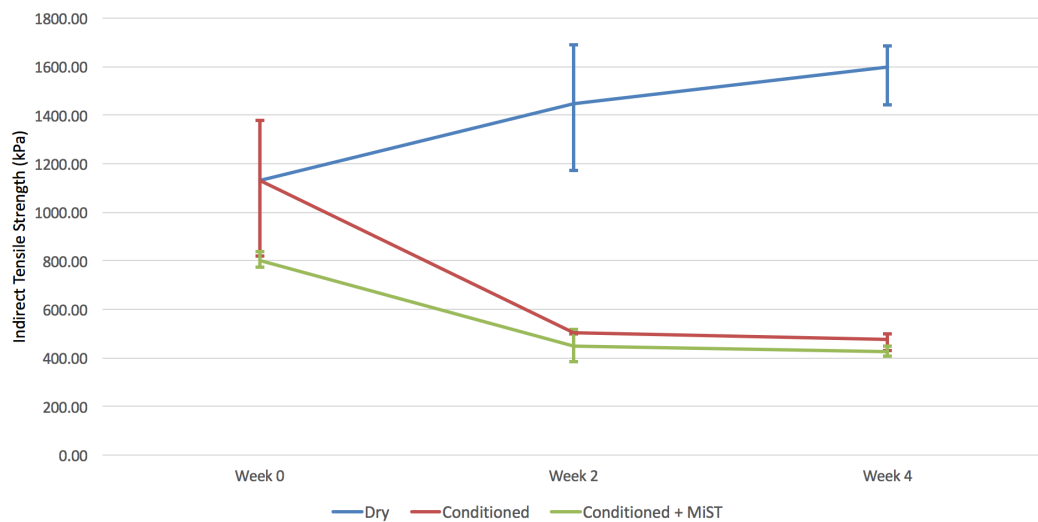


Figure 3.8: ITS for aged cores of Mixture B after conditioning and MIST

### 3.3.3. Mixture C

While performing an indirect tensile strength test on mixture C, the deformation of the specimen was more than 50mm without resulting in any visible or noticeable damage to the specimen. After unloading, the specimen showed no permanent deformation and took back its original shape. Because of this, it was decided to determine the Direct Tensile Strength (DTS), and compare these values to the Indirect Tensile Strengths of the other materials.

Pramesti [21] showed that the Indirect Tensile Strength can be compared to the Direct Tensile Strength, although there might be some divergence, which had to be kept in mind while comparing. The cores were kept in their original circular shape during the conditioning and, for those cores governing, the MIST. After this, a beam with dimensions of approximately 30x30x80mm was sawn from the core, see figure 3.9.

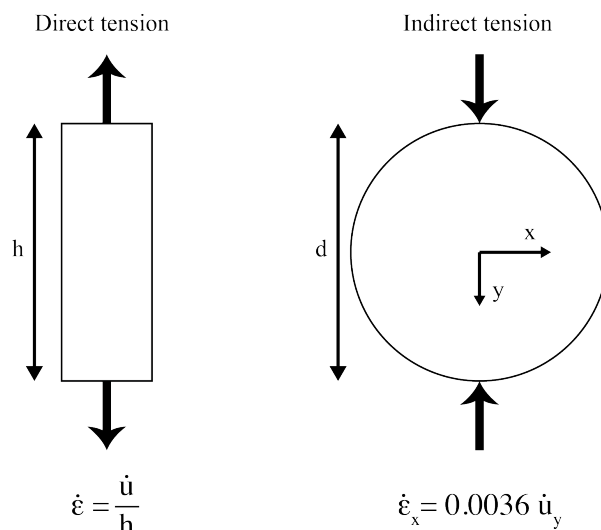


Figure 3.10: Strain rate calculations for ITT and DTT

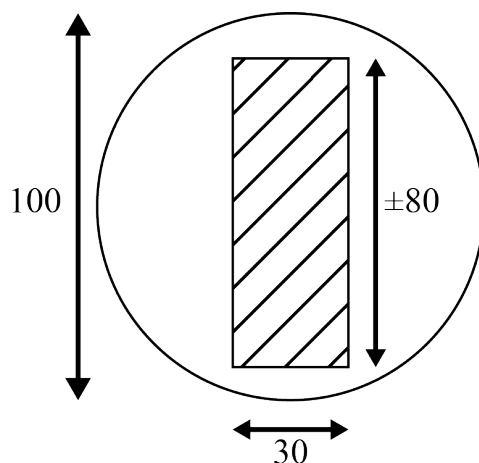


Figure 3.9: Beam sawn from 100mm core

Because of the problems due to the elasticity of the material and problems with adhesion to the caps used in the test machine for the direct tension test, some specimens failed. Those were replaced by the manufacturer, but it resulted that for the fresh subset (unaged) no cores were available for the dry reference tests every two weeks. Therefore, the dry strength was taken constant over the four weeks.

Now, in order to be able to compare those values to those of mixtures A and B, we had to convert the values. Because the vertical displacement speed for the Indirect Tensile Test had to be 50.8mm per minute according to the standards, a comparable deformation speed for the direct tensile test was needed. Erkens [22] derived the formulas for the strain rate in order to compare the ITT and DTT.

According to Erkens [22], the strain rate of the DTT can be determined by:

$$\dot{\epsilon} = \frac{\dot{u}}{h} \tag{3.1}$$

The strain rate of the ITT was more difficult, but as Erkens [22] derived, assuming a Poissons ratio of 0.33, one can use:

$$\dot{\epsilon}_x = 0.0036 \cdot \dot{u}_y \tag{3.2}$$

With the ITT's vertical displacement speed being 50.8mm/min and the beams having a height of ap-

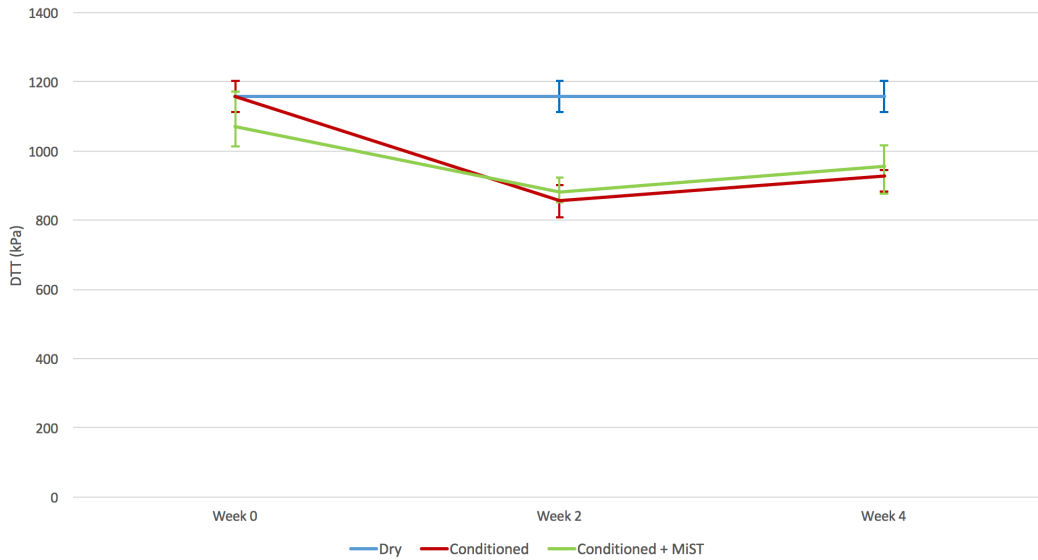


Figure 3.11: Uncorrected DTS for fresh cores of Mixture A after conditioning and MIST

proximately 80mm, this resulted in a vertical deformation speed of 14.6mm/min.

$$0.0036 * 50.8 = \frac{\dot{u}}{80} \rightarrow \dot{u} = 14.6 \quad (3.3)$$

This comes down to a reduced strain rate of:

$$\frac{14.6}{80} * 100 = 18.25\%/min = 0.3\%/s \quad (3.4)$$

During the test, the peak force at which the specimen broke, was measured. According to the Dutch standard [23], the direct tensile strength was calculated by dividing the measured tension force at failure by the initial cross sectional area of the specimen being tested. This resulted in the values shown in figures 3.11 and 3.12.

These results showed that the direct tension strength decreased a bit after 2 weeks of conditioning, but the cyclic pore pressure, applied by the MIST, did not have a great influence, again because of the capacity to deform like with Mixture B. By looking at the behaviour of the dry aged specimens, the assumption to take the dry strength for the fresh specimens as a constant can be assumed to be correct.

Because Pramesti [21] published a comparison between the Monolithic Uniaxial Tensile Test and the Indirect Tensile test at 15 degrees, I re-evaluated her raw data to make the same comparison at 20°C, as shown in figure 3.13.

Figure 3.13 shows that GAC can have a difference between indirect- and direct tensile strength of up to 15% at a temperature of 20°C and a strain rate of 0.3%/s. Assuming the same behaviour for Mixture C, we therefore had to reduce the direct tensile strength by 15% to make a fair comparison between all three mixtures. These results are shown in figures 3.14 and 3.15.

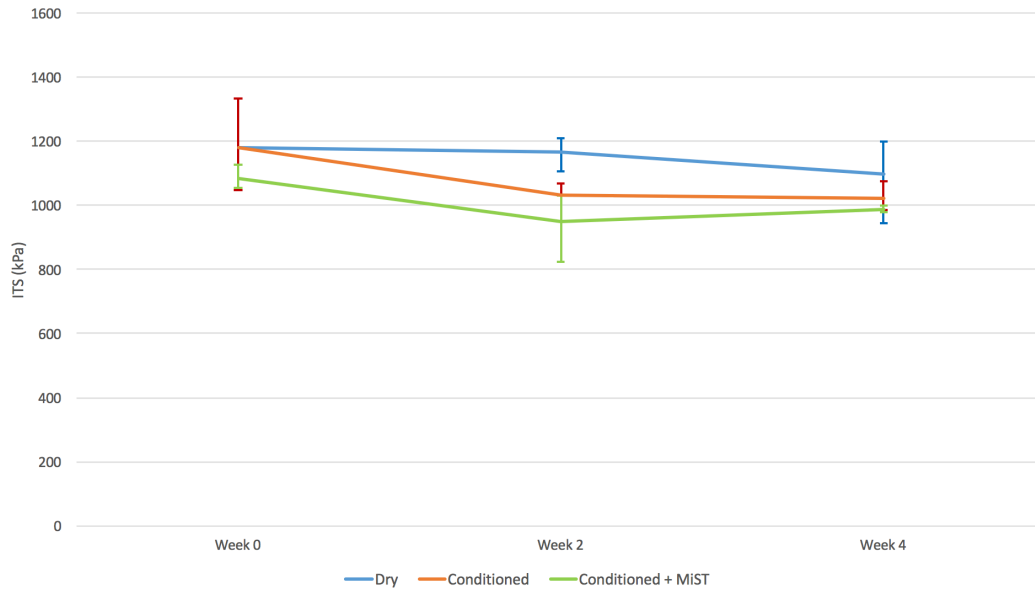


Figure 3.12: Uncorrected DTS for aged cores of Mixture A after conditioning and MIST

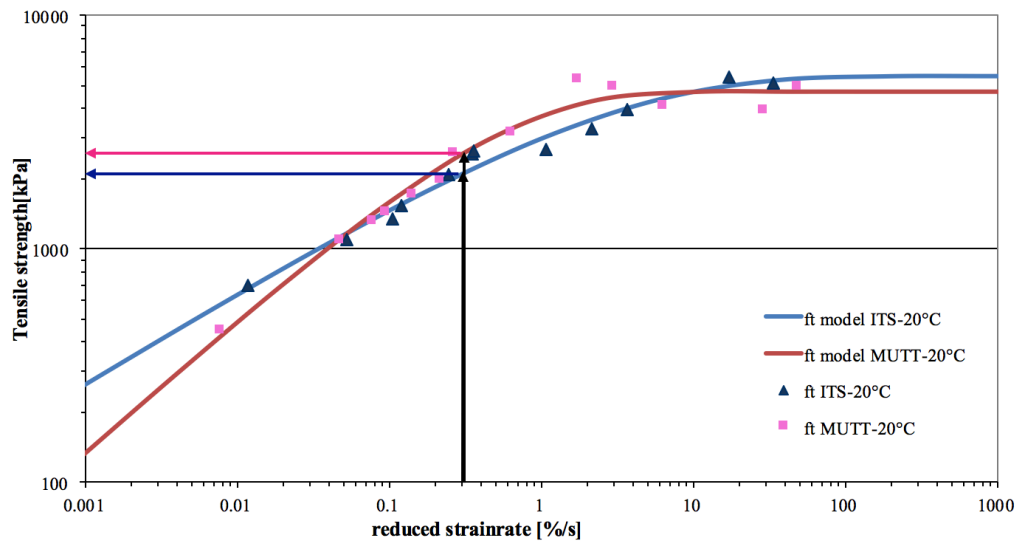


Figure 3.13: Mastercurve as made by Pramesti [21], but recalculated for 20°C

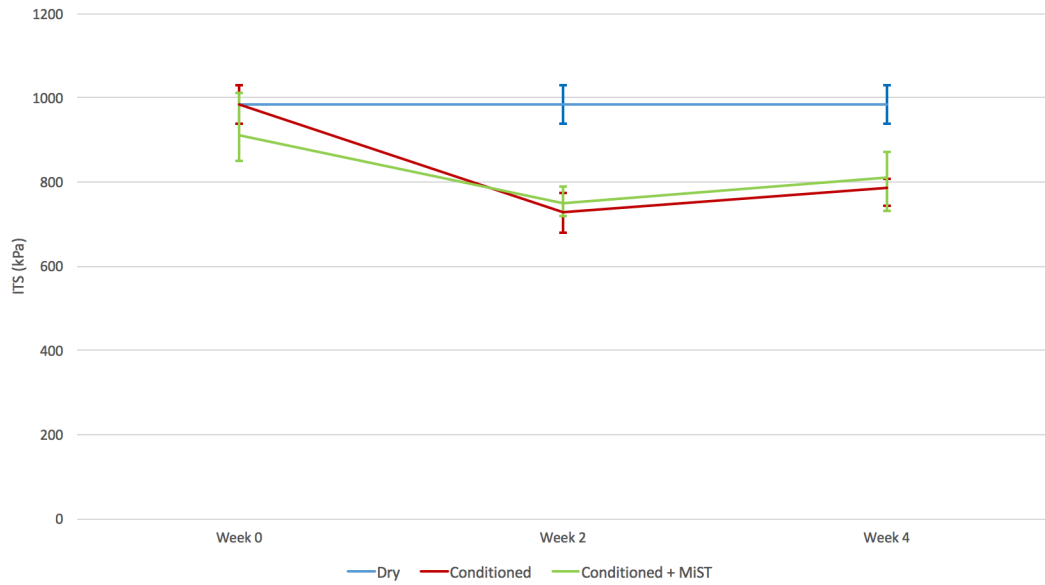


Figure 3.14: Calculated ITS for fresh cores of Mixture C after conditioning and MIST

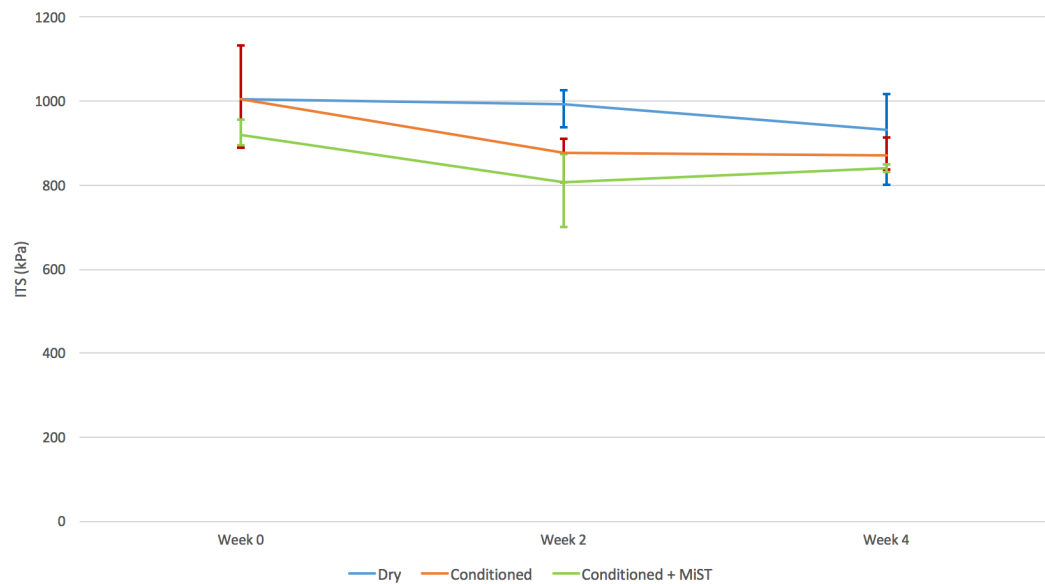


Figure 3.15: Calculated ITS for aged cores of Mixture C after conditioning and MIST

### 3.3.4. Comparison

To gain a better insight of the moisture susceptibility of the USP mixtures the Indirect Tensile Strength Ratio (ITSR) was introduced. This ITSR can be defined as:

$$ITSR(\%) = \frac{S_{wet}}{S_{dry}} \cdot 100 \quad (3.5)$$

For every mixture, the dry strength as measured in week zero was taken as  $S_{dry}$ . The tensile strength ratios for the fresh materials can be found in table 3.2 and for the aged materials in table 3.3

	0 Weeks	2 Weeks	4 Weeks
Dry	100%	101%	88%
Conditioned	-	104%	100%
Conditioned + MIST	94%	64%	54%

(a) Mixture A

	0 Weeks	2 Weeks	4 Weeks
Dry	100%	151%	169%
Conditioned	-	68 %	59%
Conditioned + MIST	78%	75%	56%

(b) Mixture B

	0 Weeks	2 Weeks	4 Weeks
Dry	100%	100%	100%
Conditioned	-	74%	80%
Conditioned + MIST	92 %	76%	82%

(c) Mixture C

Table 3.2: TSR (%) for fresh mixtures

	0 Weeks	2 Weeks	4 Weeks
Dry	100%	99%	99%
Conditioned	-	81%	96%
Conditioned + MIST	70%	54%	92%

(a) Mixture A

	0 Weeks	2 Weeks	4 Weeks
Dry	100%	128%	141%
Conditioned	-	44 %	42%
Conditioned + MIST	71%	40%	38%

(b) Mixture B

	0 Weeks	2 Weeks	4 Weeks
Dry	100%	99%	93%
Conditioned	-	87%	87%
Conditioned + MIST	92 %	80%	84%

(c) Mixture C

Table 3.3: TSR (%) for aged mixtures

### 3.4. Conclusion

For mixture A, the effect of moisture conditioning alone is not very visible. Neither is the effect of ageing. For the fresh samples, after four weeks of conditioning and applying the cyclic pore pressure, we do see a decrease in strength of 46%. For the aged samples, the strengths after four weeks are much higher than after two weeks. Maybe for these samples, the composition was different, but no information on this is available.

The first thing we see when looking at the results of mixture B is the hardening of the material over the four weeks period. By comparing the strength of the unconditioned samples in week zero and week four, we observe an increase in strength of 69% for the fresh samples and 41% for the aged samples.

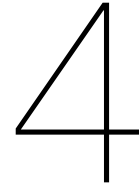
Although the increase in dry strength, there is a decrease in strength for the conditioned and conditioned + MIST samples, for both the fresh and the aged subsets. The bottom values are similar for

both subsets (a little over 400 kPa), although the strength in week zero varies.

For mixture C, the graphs are much more flattened compared to the other two mixtures. The effects of conditioning and cyclic pore pressure are much lower for this material. Also ageing in the oven does not influence the strength.

Based on these results, we can conclude that elastic mixtures like Mixture B and Mixture C, are less susceptible to damage due to cyclic pore pressure induced stresses. The stiffer Mixture A, however, proves that a lack of deformation capacity results in damage due to these cyclic pore pressures. According to the Dutch specifications based on the NEN-EN 12697-12, Method A, the ITSR of a mixture may not get below 80%. Otherwise a mixture is defined as being susceptible to moisture damage. Since the conditioning protocol used for this master thesis is more aggressive, it can be considered that an ITSR of 70% can be taken as the lower limit.

Considering the above, only Mixture C fulfils this requirement in all cases. Mixture A fails on this requirement after applying cyclic pore pressure, and Mixture B fails after the moisture conditioning in the water bath.



# Dynamic stiffness

## 4.1. Introduction and formulae

According to [24], for determination of the dynamic stiffness using a cyclic loading, one has to measure the applied load, the displacement and the phase angle between the loading and the deformation. The load and displacement were measured by the test setup, while the phase angle had to be calculated from the results.

The dynamic (complex) modulus is in [24] defined as:

$$E^* = |E^*|(\cos(\Phi) + i \sin(\Phi)) \quad (4.1)$$

where, according to [25],

$$|E^*| = \sigma_0 / \varepsilon_0 \quad (4.2)$$

From this,  $E_1$  and  $E_2$  can, according to [24] and [25], be defined as:

$$E_1 = |E^*| \times \cos(\Phi) = \frac{\sigma_0}{\varepsilon_0} \times \cos(\Phi) \quad (4.3)$$

$$E_2 = |E^*| \times \sin(\Phi) = \frac{\sigma_0}{\varepsilon_0} \times \sin(\Phi) \quad (4.4)$$

In [25], it is also written that the phase angle  $\Phi$  can be found by:

$$\Phi = \frac{t_i}{t_p} \times 360^\circ \quad (4.5)$$

where  $t_i$  is the time lag between a stress cycle and a strain cycle, and  $t_p$  is the length of a stress cycle, see figure 4.1.

To create a master curve, the reduced frequency has to be calculated. This reduced frequency is found by multiplying the test frequency by a certain shift factor  $\alpha_T$ . [26] This shift factor can be calculated in (at least) 2 ways, as described in [27]. The first method is using the Arrhenius type equation:

$$\log \alpha_T = C \left( \frac{1}{T} - \frac{1}{T_{ref}} \right) = \log e \frac{\Delta H}{R} \left( \frac{1}{T} - \frac{1}{T_{ref}} \right) \quad (4.6)$$

where:

- $T$  = the experimental temperature (K)
- $T_{ref}$  = the reference temperature (K)
- $C$  = a constant (K)
- $\Delta H$  = activation energy (J/mol)
- $R$  = ideal gas constant, 8.314 J/(mol·K)

According to [27], different values for the constant C are reported:

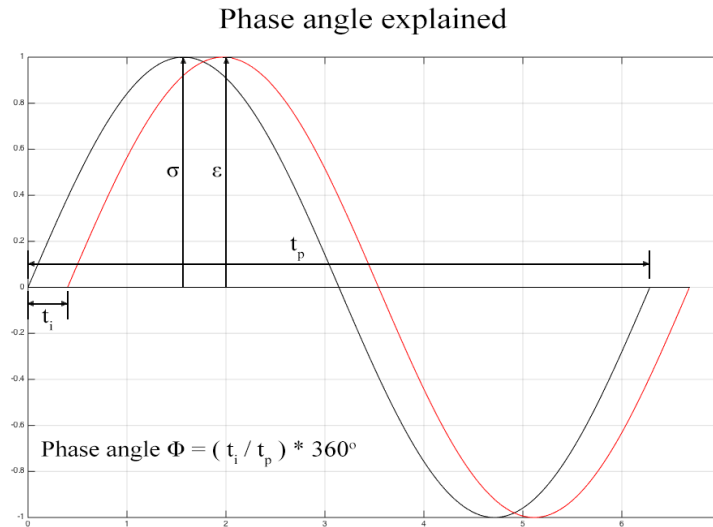


Figure 4.1: Explanation of the phase angle  $\Phi$

- $C = 10920 \text{ K} \rightarrow$  Francken et al. (1988)
- $C = 13060 \text{ K} \rightarrow$  Lytton et al. (1993)
- $C = 7680 \text{ K} \rightarrow$  Jacobs (1995)

Another way to calculate the shift factor for the reduced frequency, is using the Williams-Landel-Ferry (WLF) equation:

$$\log f_{fict} - \log f = \log \alpha_T = - \left( \frac{C_1 \cdot (T - T_{ref})}{C_2 + (T - T_{ref})} \right) \quad (4.7)$$

where:  
 $f_{fict}$  = the frequency where the master curve should be read (Hz)  
 $f$  = loading frequency (Hz)  
 $C_1, C_2$  = empirical constants

Again, according to [27], different values for  $C_1$  and  $C_2$  can be found in literature:

- $C_1 = 9.5$  and  $C_2 = 95 \rightarrow$  Sayegh (1967)
- $C_1 = 19$  and  $C_2 = 92 \rightarrow$  Lytton et al. (1993)

For this research, the Master Curve was calculated using the Arrhenius equation (4.6). The different results from the various tests were fitted manually in order to get the right reduced frequencies.

## 4.2. Test setup and sample preparation

The test were performed in a hydraulic test setup, placed in a climate cabinet. The specimens were glued into the machine and stayed there until all tests at all temperatures were performed. During the time that the temperature was being changed, a small compressive force of 15N was applied to the specimen, to compensate for the permanent deformation due to the cyclic tensile test.

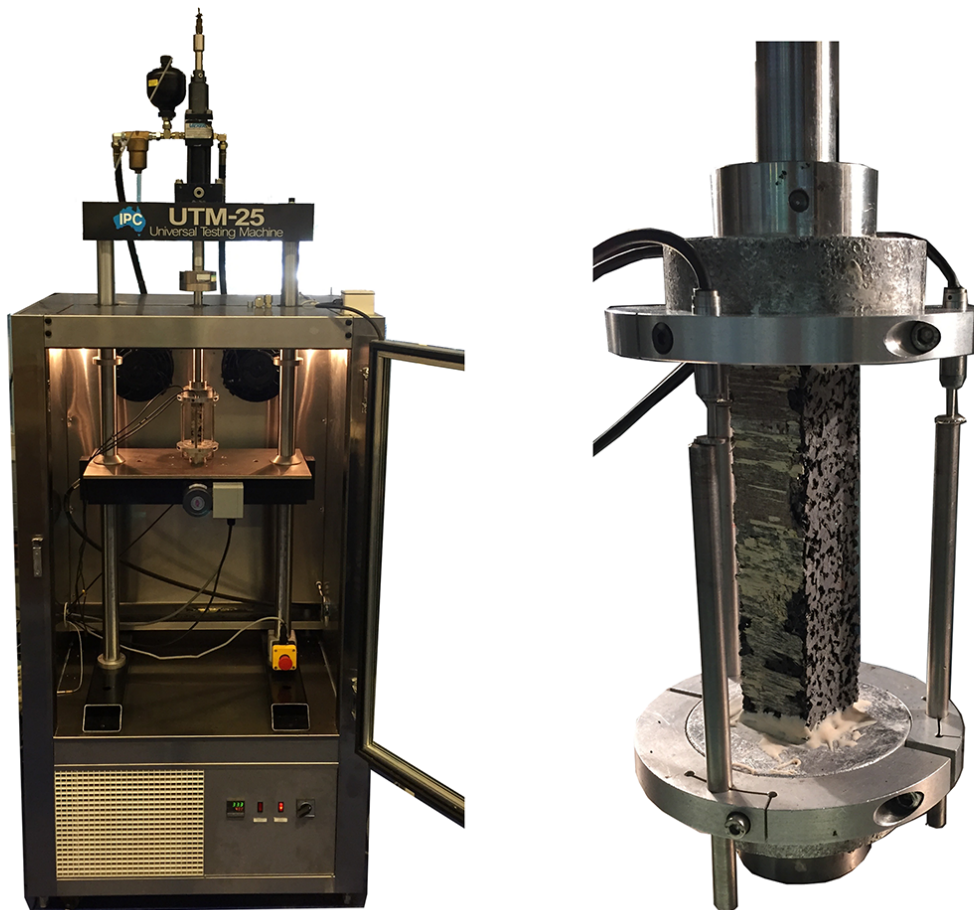


Figure 4.2: Stiffness testing cabinet (L) and sample closeup (R)

Each specimen was tested at 5 temperatures and 7 frequencies for each temperature. The test temperatures were  $-5$ ,  $5$ ,  $15$ ,  $25$  and  $40$  °C, and the frequencies were 10, 5, 2, 1, 0.5, 0.2 and 0.1 Hz.

The specimens consisted of beams with a cross section of  $\pm 30 \times 30$  mm and a length of 130 mm for mixture A, and 150 mm for mixtures B and C. This was decided because of the elasticity of the materials B and C compared to material A, and the possible boundary effects of the glue at the ends of the beams. The difference in length was compensated for the calculation of the master curve.

### 4.3. Results

While performing the tests, the output data for both the measured force and the measured displacement were not exactly sine waves, especially for the higher frequencies. This made it hard to determine the phase angles and the phase shifts as described earlier. To solve this, a Fourier analysis was performed on the raw data, resulting in a second order Fourier series as shown in figure 4.3. These series were used to calculate the phase angles and -shift.

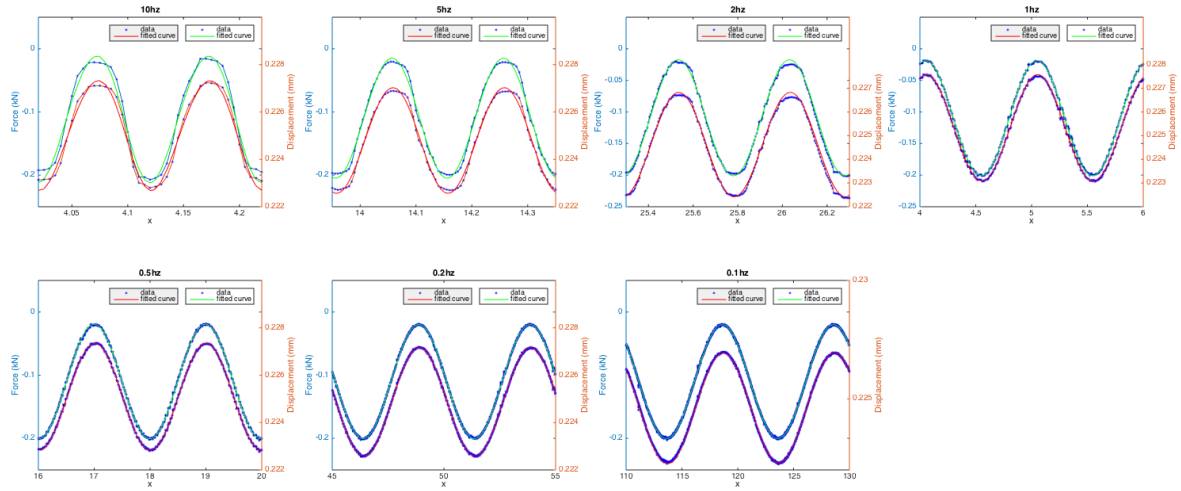


Figure 4.3: Fourier analysis performed on the raw output data of Mixture A, beam 1 at 15 °C

For each mixture, 2 fresh and 1 aged beams were tested. For the second fresh beam of material B, no information for  $T=40^{\circ}\text{C}$  was available because the test setup broke down while heating to this temperature. Therefore, the master curve for this beam is a bit inaccurate at the lower reduced frequencies, as shown in figure 4.4. The phase angles (degrees) and  $E^*$  (MPa) values can be found in tables 4.1 and 4.2. The beams noted with the subscript  $a$  are the aged beams.

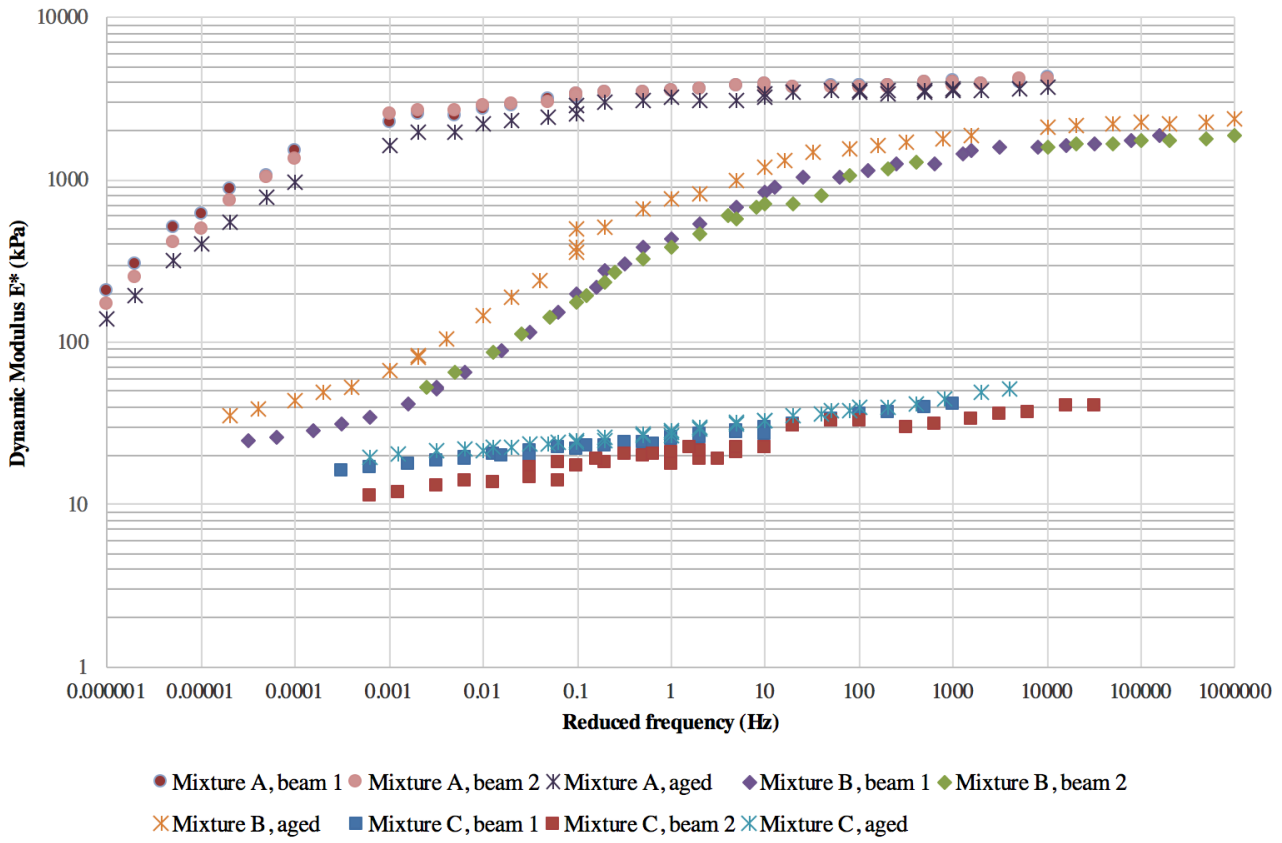


Figure 4.4: Mastercurves for mixtures A, B and C.

T(°C)	Hz	Phase Angles $\phi$								
		A1	A2	A <sub>a</sub>	B1	B2	B <sub>a</sub>	C1	C2	C <sub>a</sub>
-5	10	5.4	4.7	1.1	7.2	2.5	3.6	8.3	7.6	8.6
	5	2.7	2.7	0.2	4.3	2.3	2.0	7.7	7.2	8.5
	2	1.5	1.6	0.6	3.9	3	2.3	7.6	7.1	6.8
	1	1	1.3	0.0	4.8	4.6	2.3	9.5	8.9	8.4
	0.5	0.9	1	0.6	4.1	3.8	2.4	8.5	8	8.4
	0.2	0.9	1.1	0.6	7.3	6.2	3.1	8.2	7.5	7.8
	0.1	0.9	1	0.6	6.8	6.6	3.3	7.8	7.3	7.4
5	10	4.7	4.3	2.2	11.2	10.4	4.3	7.2	6.8	7.6
	5	2.5	2.5	0.7	10.8	6.3	5.6	6.8	6.3	7.6
	2	1.4	2.3	0.6	13.2	8.6	6.3	6.3	6.2	6.0
	1	0.9	1.2	0	12.3	14.1	7.8	8.2	12	7.3
	0.5	0.6	1	0.4	9.2	12.3	8.6	7.5	10.7	7.2
	0.2	0.7	1.2	0.5	19.8	21.7	12.6	7.3	10.7	6.9
	0.1	0.9	1.2	0.5	20.2	21.6	13.4	7	10.5	6.3
15	10	4.7	4.7	1.4	22.3	20.9	10.1	6.1	6.1	6.1
	5	2.9	3.1	0.2	18.9	14.8	11.2	6.3	6.8	6.1
	2	2.2	2.1	0.7	20.7	19.8	16.7	5.9	7.1	6.0
	1	2.2	2	2.4	30.8	30.6	25.1	6.5	9.4	6.2
	0.5	1.7	1.7	2.0	26.9	28.6	21.9	6.1	8.9	6.5
	0.2	2.5	2.2	3.4	36.6	34	33.1	6.7	8.8	6.1
	0.1	2.7	2.3	3.4	35.3	32.6	32.5	6.3	8.9	5.6
25	10	8.6	7.2	2.9	27.7	23	20.5	5.4	0	5.4
	5	7.7	6.1	3.2	28.6	25	22.7	5.9	7	5.8
	2	8.1	6	6.3	29.6	27.6	28.6	5.4	5.9	5.5
	1	9.3	7.3	11.1	35.8	33.4	37.3	6.6	8.1	6.3
	0.5	7.1	6	8.9	30.9	28.7	32.9	6.5	7.5	6.3
	0.2	14.6	11.1	18.8	25.3	23.4	28.7	6.2	7.3	6.0
	0.1	15.9	12.3	18.3	21	19.5	24.7	6.1	7.4	5.5
40	10	27.7	25.9	16.6	19.4	0	17.6	5.4	10.1	4.3
	5	29.2	27.9	19.4	14.8	0	18.4	5.9	8.1	5.0
	2	26.6	29.2	27.7	11.4	0	15.7	5.5	7.2	5.3
	1	39.7	45.4	44.2	11.2	0	15.7	6.9	8.9	5.8
	0.5	38	40.1	38.2	8.7	0	12.1	6.6	7.8	6.0
	0.2	43.5	43.2	39.0	6.3	0	8.9	6.5	7.6	5.8
	0.1	40.9	39.4	36.2	5.1	0	6.8	6.5	7.7	5.5

Table 4.1: Phase angles

T(°C)	Hz	Dynamic Modulus E*								
		A1	A2	A <sub>α</sub>	B1	B2	B <sub>α</sub>	C1	C2	C <sub>α</sub>
-5	10	3586	3531	3745	1871	1869	2379	36	36	52
	5	3372	3472	3653	1738	1780	2248	35	35	49
	2	3284	3291	3593	1662	1735	2224	32	32	45
	1	3255	3193	3570	1637	1730	2244	31	31	42
	0.5	3227	3157	3587	1577	1666	2205	29	30	40
	0.2	3192	3133	3545	1584	1648	2178	27	28	38
	0.1	3178	3102	3467	1502	1589	2128	26	26	36
5	10	3436	3361	3659	1450	1282	1870	30	29	39
	5	3360	3313	3499	1261	1163	1787	29	29	38
	2	3201	3189	3410	1269	1061	1722	27	27	35
	1	3190	3135	3556	1134	794	1631	26	20	33
	0.5	3151	3100	3523	1031	711	1538	25	18	32
	0.2	3118	3084	3474	1038	681	1470	23	17	30
	0.1	3098	3057	3424	892	600	1330	22	16	29
15	10	3241	3231	3201	833	715	1208	24	19	33
	5	3188	3190	3111	683	570	990	24	20	31
	2	3006	3011	3064	539	464	829	23	19	30
	1	2937	2965	3198	434	381	768	22	18	28
	0.5	2878	2913	3077	387	324	661	21	17	27
	0.2	2859	2886	3014	277	235	515	20	16	26
	0.1	2815	2839	2871	200	175	382	19	15	25
25	10	2697	2759	2532	306	269	497	21	17	27
	5	2660	2512	2426	219	196	355	21	19	26
	2	2368	2469	2341	152	142	241	20	18	25
	1	2273	2403	2209	114	111	190	19	18	24
	0.5	2097	2250	1962	90	87	147	19	17	24
	0.2	2108	2246	1959	65	65	105	18	16	22
	0.1	1905	2103	1615	53	53	83	17	15	22
40	10	1264	1123	968	51	-	81	17	12	24
	5	880	870	783	41	-	67	17	13	24
	2	728	615	553	34	-	53	16	12	23
	1	515	417	406	32	-	49	16	12	22
	0.5	423	347	315	29	-	44	15	11	22
	0.2	256	209	195	26	-	38	15	10	21
	0.1	175	144	138	25	-	36	14	10	20

Table 4.2: Dynamic modulus values

## 4.4. Conclusion

It is clear from the master curves that Mixture A is the stiffest, Mixture B follows and Mixture C is the most flexible. For Mixture A can be seen that, especially for the lower reduced frequencies, the graph is very steep. This means that its behaviour when applied in the field, can become unpredictable on the few hottest days during its lifetime. For the average and higher reduced frequencies, the behaviour is almost constant, but the dynamic modulus is too high. This results in problems as seen with the cyclic pore pressure loading.

Ageing did not have much influence on the stiffness of Mixture A. The stiffness even decreased a bit, but for the flattest part of the master curve, there is not much difference between the aged and the unaged beams.

The graph of Mixture B has the steep part in the master curve around the average reduced frequencies, which are the normal loading frequencies at the reference temperature ( $15^{\circ}\text{C}$ ). The difference in dynamic modulus between the higher and lower reduced frequencies indicates the great susceptibility to changes in temperature or loading frequencies.

For this mixture the effect of ageing is the most present, however further research is necessary to determine the cause of this. As shown with the indirect tension test (ITT), this material already hardened in 4 weeks at  $15^{\circ}\text{C}$  in a storage chamber. For example, it can also be possible that the binder is not fully hardened for the unaged beams.

Mixture C is almost constant over the full range of the reduced frequencies, indicating an almost fully elastic behaviour. This behaviour is favourable, since the occurring stresses due to traffic loading will be almost constant for all traffic loading scenarios and occurring temperatures.

Ageing hardly affected the stiffness of Mixture C.

# 5

## Interlayer bonding, using the Tensile Adhesion Test (TAT)

### 5.1. Introduction

From previous field tests, one of the main problems seemed to be the bond of the PERS with the underlying layers. On the test at the Dutch A50, the pavement was immersed with water for a few months and after that, not only the strength of the PERS, but also the bond strength with the asphalt below decreased [9]. Therefore, the effect of moisture conditioning on the bond strength had to be investigated.

### 5.2. Testing procedure and apparatus

Before the start of this master thesis, it was already decided that the bond strength of the PERS with an underlying layer of porous asphalt (PA) would be tested using a uniaxial tensile test (pull-off).

For each mixture, we had a 50x50x8cm slab, made of two layers of asphalt: 50mm PA and 30mm PERS. 12 50mm cores were drilled from each slab. For Mixture B, this gave some problems because the cores were hard to get out of the drill, or stuck with the porous asphalt part to the cast. This resulted in breaking of some of the cores while taking them out. However: We did get 12 good cores for the tests.



Figure 5.1: The 3 mixtures after coring the 50mm cores.

For the conditioning, the same water bath used for the indirect tensile strength tests was used and again at a temperature of 60°C. The conditioning was performed over a total period of six weeks: For each material, three cores were not conditioned and the others were placed in the bath. After every period of two weeks, three cores of each mixture were taken out and stored in a climate chamber.



Figure 5.2: Cores in the conditioning bath. Note that two cores of Mixture B are orientated in a different direction. This is because the raster of cores was what kept the cores upright. Since those 2 were not in the raster, they were placed flat so that they would not wobble around by the currents in the bath.

When the conditioning was done, the cores were glued between two aluminium caps that could be connected to the test setup. For the execution of the test, we had 2 options: Taking the vertical displacement speed as input parameter, like described in the NEN-EN 12697-46 [23], or taking the measured force as input parameter as described by Raab and Partl in [28] according to the German specification ZTV-SIB 90. In the preliminary phase of the research on PERS at TU Delft, this same test was done using the vertical displacement as input parameter, so that is why it was decided to use that for this test as well. This speed was taken as 50.8mm/min.

The testing setup consisted of a climate cabinet containing a pneumatic, single axis test frame. The same frame was used for the ITT but instead of operating in compression, we now tested on tension. A photo of the setup is shown in figure 5.3.

### 5.3. Results

While testing, it turned out to be difficult to glue the PA part of the core to the cap. This was solved by using 3D printed rings in which a pool of glue was created. This resulted in a greater contact area between the PA and the glue, because the glue became also attached to the first 8-10mm of the outer surface of the core.

For Mixture B, during the conditioning already 4 of the cores delaminated without applying any external force. Three others broke while setting up the test, also without any external force but gravity. This resulted in only two conditioned cores that could be tested. One of these was two weeks conditioned, the other one six weeks.

The manufacturer of this PERS told us that this problem might be caused by the forces exerted while coring and found another way of coring the specimens. Since there was no time to start a 6 weeks conditioning process all over, it was decided to test three dry specimens to see if there was any noticeable difference compared to the original unconditioned cores. This was not the case, so an extra conditioning period was not started.

The unconditioned cores of mixture C were the only cores that had a bond layer that was strong enough to make the cores fail on the cohesive strength of the PA instead of on the strength of the adhesion layer. However, already after two weeks of conditioning, the failure mechanism changed to adhesive failure of the interface layer.

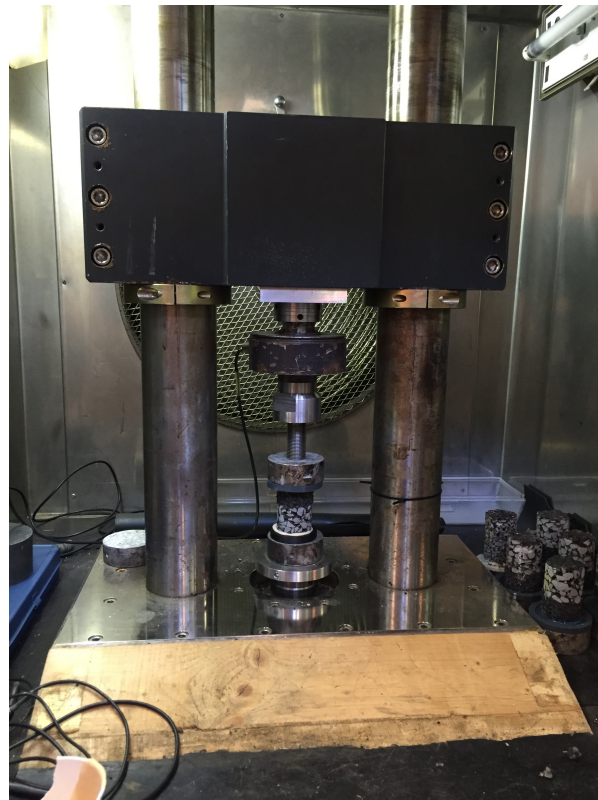


Figure 5.3: Specimen in the testing setup

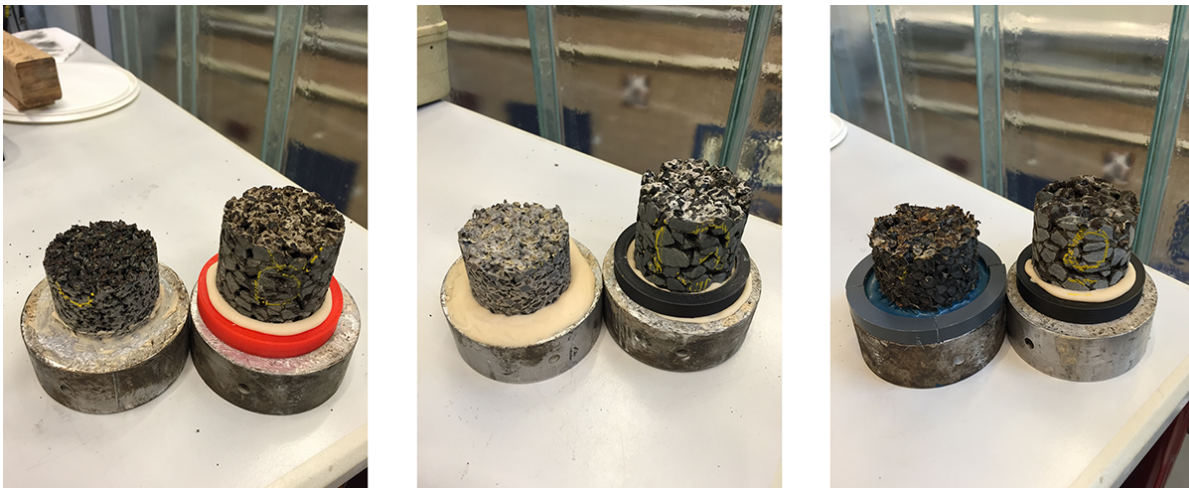


Figure 5.4: Failed TAT cores for mixtures A, B and C

	0 Weeks	2 Weeks	4 Weeks	6 weeks
Mixture A	0.66	0.46	0.22	0.17
Mixture B	0.67	0.08*	-	0.07*
Mixture C	0.87	0.69	0.62	0.55

\*Result based on only 1 test

Table 5.1: Pull-off strengths in N/mm<sup>2</sup>, averages of 3 tests

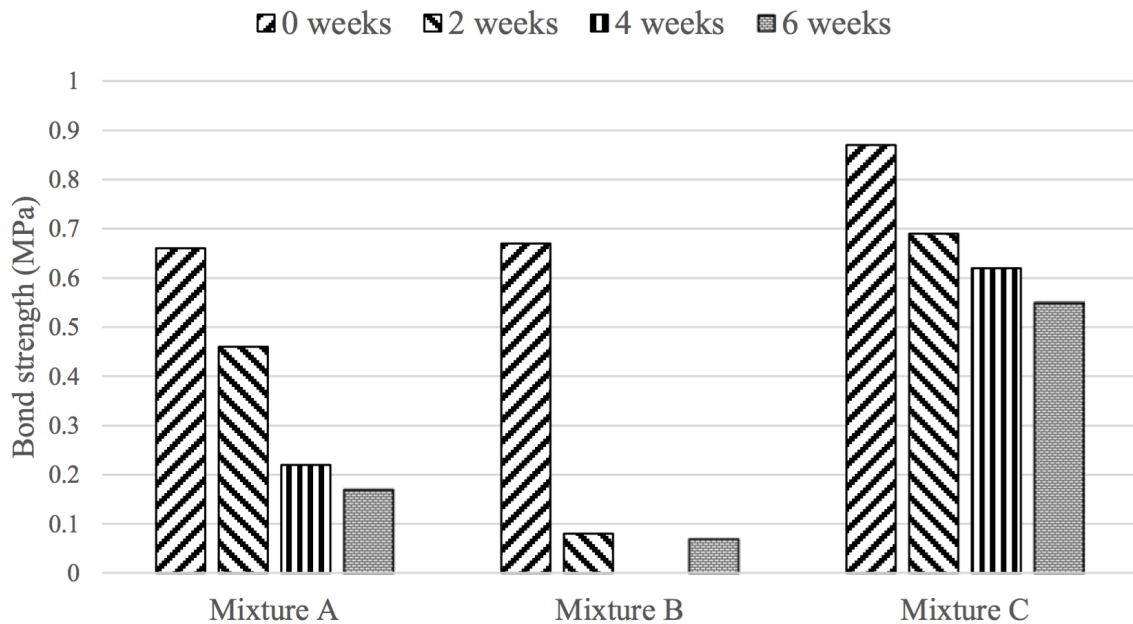


Figure 5.5: Tensile adhesion strength after moisture conditioning

In table 5.1, the average pull-off strengths of each mixture can be found. These are the averages of - when it was possible - 3 tests and are presented in N/mm<sup>2</sup>. These values are also shown in figure 5.5.

## 5.4. Conclusion

From the results, we can conclude that all mixtures are susceptible to moisture in terms of adhesion to porous asphalt. However, the bond between Mixture B and the PA is so weak that it is almost not possible to measure it. Both mixtures A and C showed a decrease in adhesion strength, but especially for mixture A this decrease is very high. Due to the high amount of air voids in the USP, water permeates easily into the pavement and affects the glue on the interface.

The problem of the adhesion between the porous asphalt and the USP is probably the great difference in particle size and the high amount of air voids of both materials, resulting in a very small contact area between the two layers. Also when glueing the porous asphalt into the test setup, the contact area between the porous asphalt and the setup turned out to be too small. This was solved by filling the porous asphalt up to 8mm with glue, but this can not be done on the interface between the porous asphalt and the USP, because this will negatively influence the permeability of the pavement.

Because of the bad results with these fresh materials, it is decided not to perform this test on aged specimens.

# 6

## Cohesive strength

### 6.1. Introduction

To get more information about the material's properties, a cohesive strength test was performed. Using a uniaxial direct tensile strength test, the strength of each material at two different temperatures and two different strain rates was determined.

### 6.2. Test setup and specimen preparation

For the cohesive strength test, beams of 30x30x130mm were used. These beams are sawn from slabs, provided by the 3 companies. For each material we needed 12 beams. With this amount, four sets of three beams could be tested at the varying temperatures and strain rates.



Figure 6.1: Test setup for determination of cohesive strength

Because of the used materials, sawing the beams did not result in beam with a perfect square cross section. Rubber particles at the bottom of the slab where just 'pushed away' and moved back when the saw was gone, resulting in non right-angled corners. Therefore, a glueing mould could not be used to glue the beams to the caps that were used to fit the beams in the test setup. To solve this problem, the beams were glued onto a cap with fast hardening glue while being hold upright.

This way of glueing did not cover the exact position of the beam on the cap, so it could not be guaranteed that there was no eccentricity. For the reason, it was decided to apply no hinges in the test setup. By applying no hinges in the test setup, the beam, with only one cap glued onto it, could be placed in the machine and was then glued to a cap in the bottom end of the machine. This resulted in a setup where the surfaces of the caps where exactly parallel to each other with the beam glued right-angled to one of them, and therefore also to the other cap. The eccentricity was now no longer a problem, and applying hinges in the setup would result in possible bending moments in the beams. A picture of the test setup is shown in figure 6.1.

The test temperatures were taken as:

- 5 °C
- 20 °C

For the strain rates, we used the displacement speed as stated in the NEN standard: 81.25mm/min [23]. For the second displacement speed, we decided to calculate this in the same way as we did with the Indirect Tensile Strength Test. As described by Erkens, a relation between the ITT's vertical displacement-, and the direct tension vertical displacement speed can be found [22]. With the same calculation as we did for the ITT, but now for 130mm beams, we found a second displacement speed of 23.8mm/min.

### 6.3. Results

As with all the tests so far, also this cohesive test showed the difference in stiffness between the mixtures. For mixture A, the graphs showed a very steep and short peak force, while for the mixtures B and C, those graphs are more rounded and less stiff. Typical graphs for the 3 different mixtures are shown in figure 6.2. Note that for mixture C, the x-axis covers 120 seconds, while this is only 40 seconds for mixtures A and B.

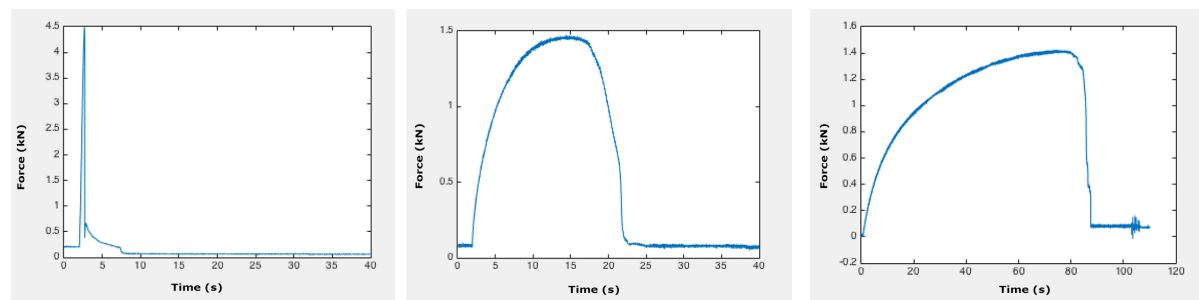


Figure 6.2: Typical behaviour for each mixture at 20°C and a displacement of 23.8mm/min. Note the different span of the x-axis for mixture C.

Some specimens did not break exactly in the middle of the beam. This was expected since the cross section of the beam was constant over the height. Therefore it was decided that when a beam broke close to one of the edges, but the force was not more than 5% different from other measurements, it was a correct test.

Table 6.1 shows the strengths of each PERS mixture under different conditions.

	Mixture A	Mixture B	Mixture C
81.3mm/min @ 20°C	4.93	1.55	1.51
23.8mm/min @ 20°C	4.64	1.41	1.36
81.3mm/min @ 5°C	4.06	3.09*	1.34
23.8mm/min @ 5°C	4.14	2.25	1.28

\*Result based on only 2 tests

Table 6.1: Cohesive strengths in N/mm<sup>2</sup>, averages of 3 tests

## 6.4. Conclusion

Mixtures A and C don't have many different outcomes for the various tests. This was expected after looking at the master curves that were created in chapter 4. In these master curves, both mixtures A and C behave almost fully elastic around the average reduced frequencies. Therefore it is not strange that the results of this cohesive strength test are not too different from each other.

Mixture B shows a clear increase in strength for both higher strain rate and lower temperatures. This indicates a stiffer behaviour at lower temperatures, which is exactly what is already concluded from the stiffness test in chapter 4.



# 7

## Finite Element Analysis: Moisture diffusion

### 7.1. Introduction

To explain the laboratory results, modern computational methods might be a good solution. As already shown by Varveri and explained in chapter 2, the effects of various moisture diffusion coefficients can be simulated by finite element methods [12]. For this master thesis, CT scans were available of prismatic specimens, so the exact same investigation as Varveri did cannot be done. The scans were made from 30x30x100mm beams, from which a cubic element of 20x20x20mm was taken for FE analysis. Such a model is shown in figure 7.1.

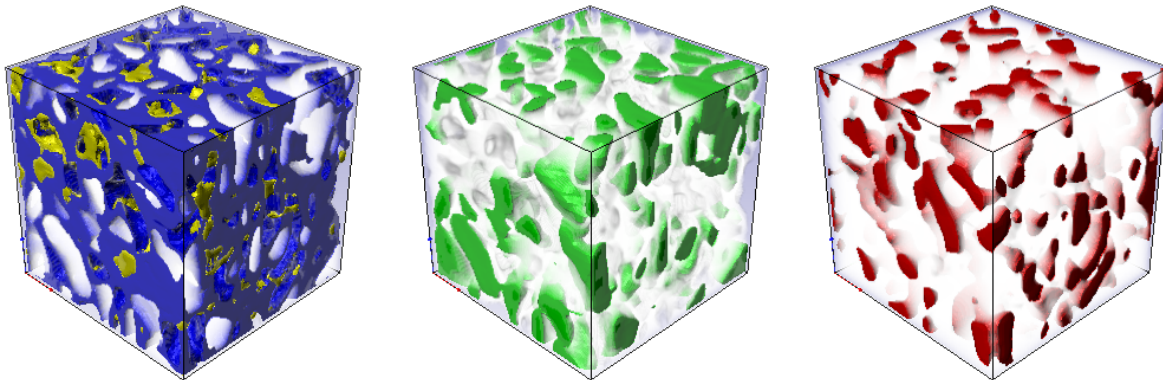


Figure 7.1: Cubic element after CT scanning showing (a) the rubber (yellow) and binder (blue), (b) the aggregates and (c) the air voids of the material.

Values for the moisture diffusion coefficients of the various materials are taken from literature:

- In [29] we find a low PU Moisture Diffusion coefficient of  $0.00760 \text{ mm}^2/\text{hour}$ .
- In [30] we find a high PU Moisture Diffusion coefficient of  $7560 \text{ mm}^2/\text{hour}$ .
- In [31], for granite, we find the Moisture Diffusion coefficient being  $0.00504 \text{ mm}^2/\text{hour}$ .
- In [32] the Moisture Diffusion coefficient for air voids is found, being  $93600 \text{ mm}^2/\text{hour}$ .

### 7.2. Creating the mesh

To create the mesh, a beam of each material was scanned using a CT-scanner. This resulted in slides of the beam which were connected to each other to generate a three dimensional image like the one shown in figure 7.2.

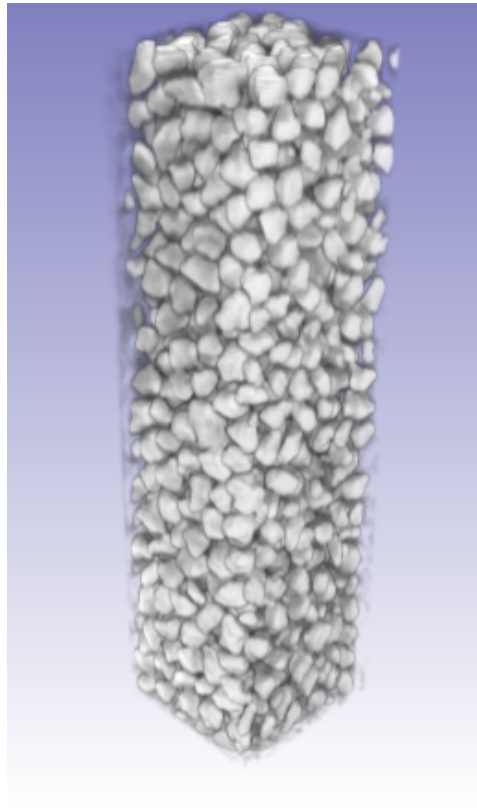


Figure 7.2: CT scan of Mixture C

From this beam, a cubicle of 20x20x20mm was taken to cut off any edge effects. Now, depending on the grayscale of the images of every slide, a material had to be assigned to the color. Since air does not reflect any radiation, the voids showed up as the darkest parts of the slice. The aggregates were the most dense materials, so they showed up brightest. A slice of the beam shown in figure 7.2 is shown in figure 7.3.

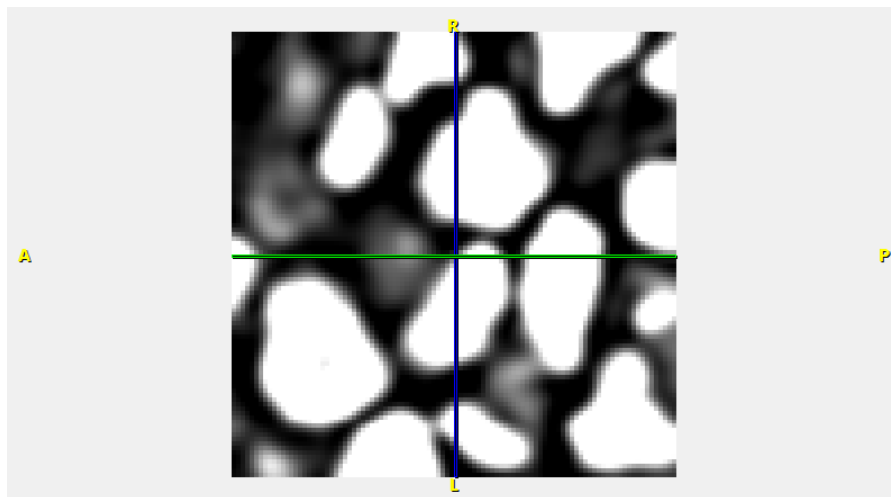


Figure 7.3: A slice of the beam shown in figure 7.2

Now in this image, it is hard to distinguish the rubber and the binder. Because every aggregate was enrobed with rubber, the small, grey line around every aggregate was assigned to be rubber, and everything between rubber and void was assumed to be binder.

To make this graphically a bit more clear, each material was assigned a certain colour, as shown

in figure 7.4.

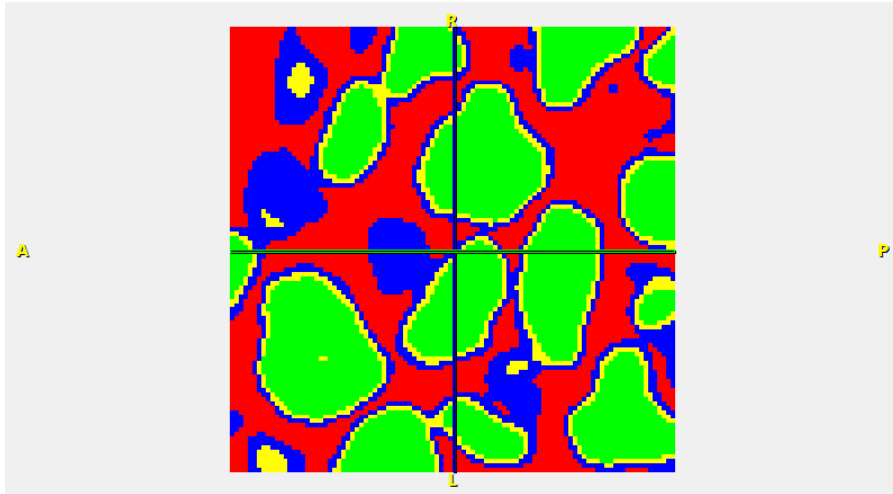


Figure 7.4: Coloured based on greyscale

Now, the same colours can be assigned to the grayscale's of all slices, which will result in a coloured 3D cube, shown in figure 7.5.

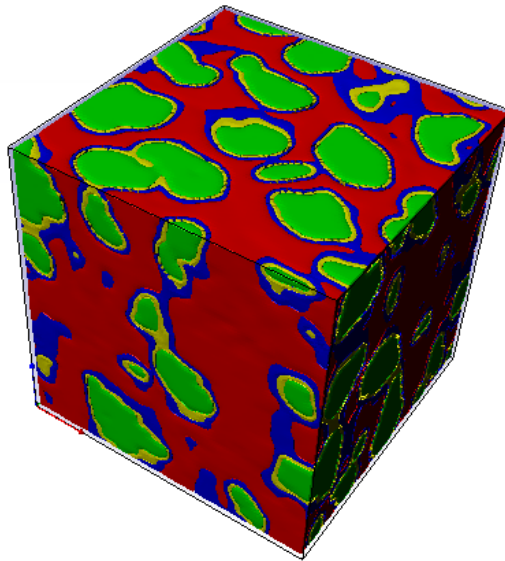


Figure 7.5: Coloured 3D cube of mixture C

With this model, it was also possible to only enable 1 of the colours, like shown in figure 7.6 where only the aggregates of the cube are shown.

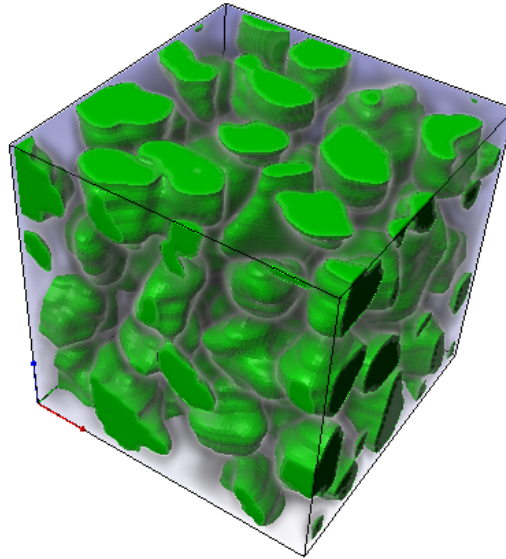


Figure 7.6: Only the aggregates of mixture C

Now from these models, a mesh could be generated. For this research, a mesh consisting of tetrahedral elements was made and used, and with the chosen element size this resulted in 1.5-2.0 million triangles per mixture. The mesh belonging to the cubes above is shown in figure 7.7.

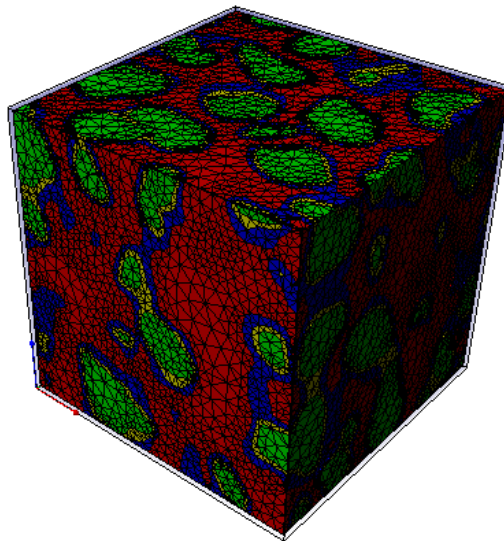


Figure 7.7: Final mesh

### 7.3. FEM input

None of the moisture diffusion coefficient of any of the materials was known, so information on this had to be taken from literature. For aggregates, air voids and the rubber this was not too difficult. For the epoxy, a lot of different values were found. The moisture diffusion coefficient really depends on the type of epoxy. This gave us the idea to see what differences a "high" and a "low" moisture diffusion coefficient had on the three mixtures. Therefore, every mixture was tested twice: with a high and a low moisture diffusion coefficient for the binder. All other input parameters were kept constant.

The input variables and model boundaries:

- The back, top and left plane of the cube are fully saturated at  $t = 0$
- A string of elements from top to bottom in the middle of the x-y plane (horizontal) is investigated over time
- The model simulates 3 weeks with output intervals of 10 hours.

## 7.4. Results

In all results, some places are already fully saturated at the lowest time interval (10 hours). This was because there was an air void at that location. In general, the aggregates saturate the slowest, since they have the lowest moisture diffusion coefficient. We focussed on their saturation speed, because we saw that the binder acted as a 'cover' for the aggregates. With a less permeable binder, the saturation speed of the aggregates was therefore much lower.

### 7.4.1. Mixture A

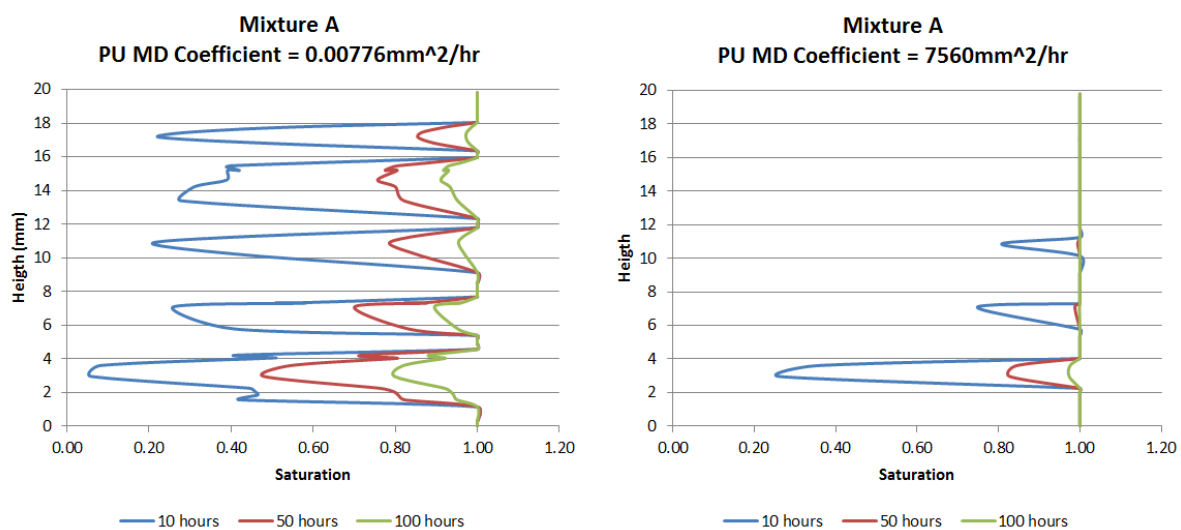


Figure 7.8: FE Results for Mixture A

In figure 7.8 we see the effects of a low and a high moisture diffusion coefficient on the mesh of mixture A. There was a great difference between those two graphs, proving that the moisture diffusion coefficient had a great influence. For the low moisture diffusion coefficient, even after 100 hours, quite some not fully saturated elements were left, while for the high moisture diffusion coefficient, almost everything was already fully saturated after 50 hours.

### 7.4.2. Mixture B

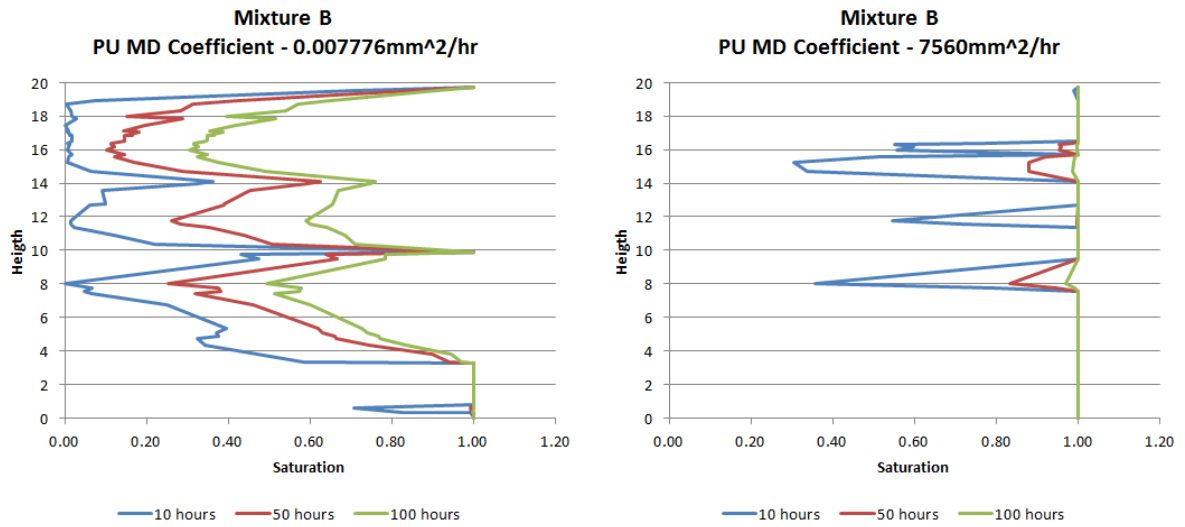


Figure 7.9: FE Results for Mixture B

For mixture B (figure 7.9) we saw the same behaviour as for mixture A, but now it seemed that the saturation speed with the lower moisture diffusion coefficient was much slower than it was for mixture A. For the high moisture diffusion coefficient, we saw the exact same behaviour.

### 7.4.3. Mixture C

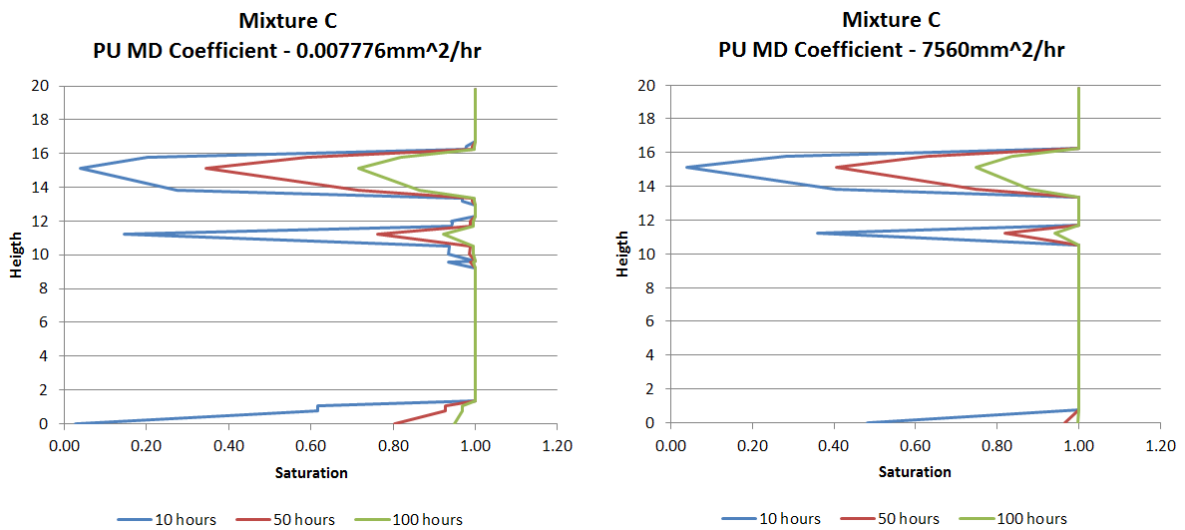


Figure 7.10: FE Results for Mixture C

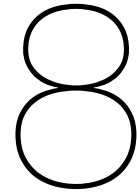
For Mixture C, the effects of a varying moisture diffusion coefficient were much lower. There was hardly any difference in saturation speed between the high and the low moisture diffusion coefficient. The mixture design of this mixture was such that the varying moisture diffusion coefficient did not affect the saturation speed.

## 7.5. Conclusion

Not only the choice for materials, but also the mixture design is of influence on the saturation speed of a mixture. While mixtures B and C have a similar amount of air voids, the saturation speed is of a different order. Also the number of air voids is of influence on the speed of saturation. Since this number is very high for Mixture A and quite lower for mixtures B and C, the difference in saturation speed can be at least partly assigned to this difference in air void percentage.

More research on the exact reasons of the varying effects of a varying moisture diffusion coefficient is needed to take a real conclusion from these results. However, for Mixture C, which contains aggregates enrobed in rubber, the higher moisture diffusion coefficient does not speed up the saturation of the material. Possibly here the rubber isolates the aggregates and protects them from the water.





# Finite Element Analysis: Moving wheel-load

## 8.1. Introduction

During the preliminary research of this project, a finite element analysis was done to see the effects of various material stiffnesses on the road structure. Now, with the stiffness of the materials known, it was possible to do this the other way around and check what the occurring stresses and strains in a road structure would be.

## 8.2. Mesh generation

The mesh made for this FE analysis was similar like the one used during the preliminary phase. This construction is shown in figure 8.1.

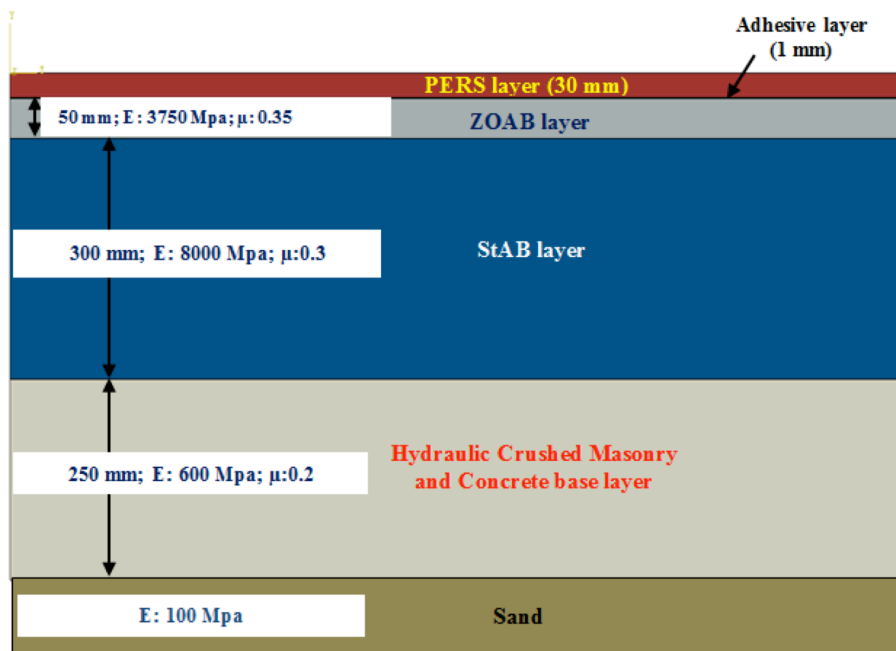


Figure 8.1: Road structure as used in the preliminary research [19]

Due to time limitations, for this master thesis, no interface layer was applied. By investigation of the occurring stresses at the bottom of the USP layer, enough information had to be collected to see the

effects of a varying stiffness in the top layer.

Also because of time limitations, FE analysis was only done for mixtures A and C. By using these two mixtures, the differences between a very flexible and a very stiff top layer were shown. With the in Chapter 4 measured complex modulus and phase angles of this material, a Prony series was made. A Prony series is a method to write a certain function as a function of 1 or more sine functions. Since we were dealing with a viscous-elastic material, the viscous property has to be taken into account. This is what the Prony method does.

Apart from the top USP layer, all other materials were defined as fully elastic, with a modulus shown in figure 8.1.

The nodes at the bottom of the USP layer were selected for output. We took a full-width strip of all nodes exactly at the middle of the structure.

### **8.3. Load**

In the preliminary phase, a wheel according with the specifications of a Goodyear 295/75 R 22.5 radial tire was used. Here, various tyre pressures, axle loads and moving speeds were investigated, but in this master thesis, this was limited to 1 situation. Since the dimensions of the wheel patch were not available, a wheel patch of 400x150mm was taken, with a pressure of 420 kPa and a moving speed of 22m/s.

### **8.4. Results**

The output of the FE analysis is shown in figures 8.2 to 8.4.

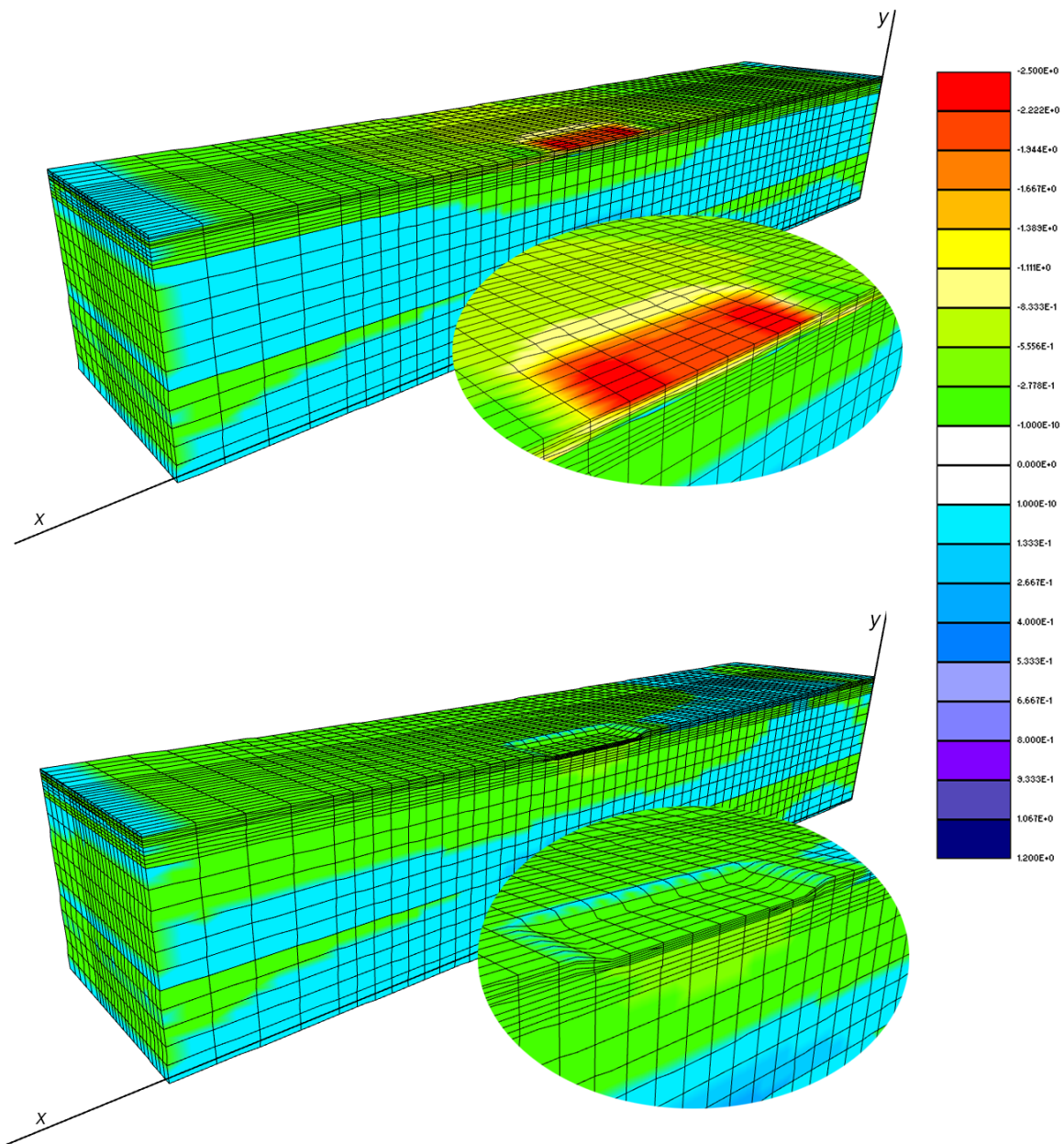


Figure 8.2: Enhanced displacement under the load and stresses ( $\sigma_{xx}$ ) for Mixture A (top) and Mixture C (bottom)

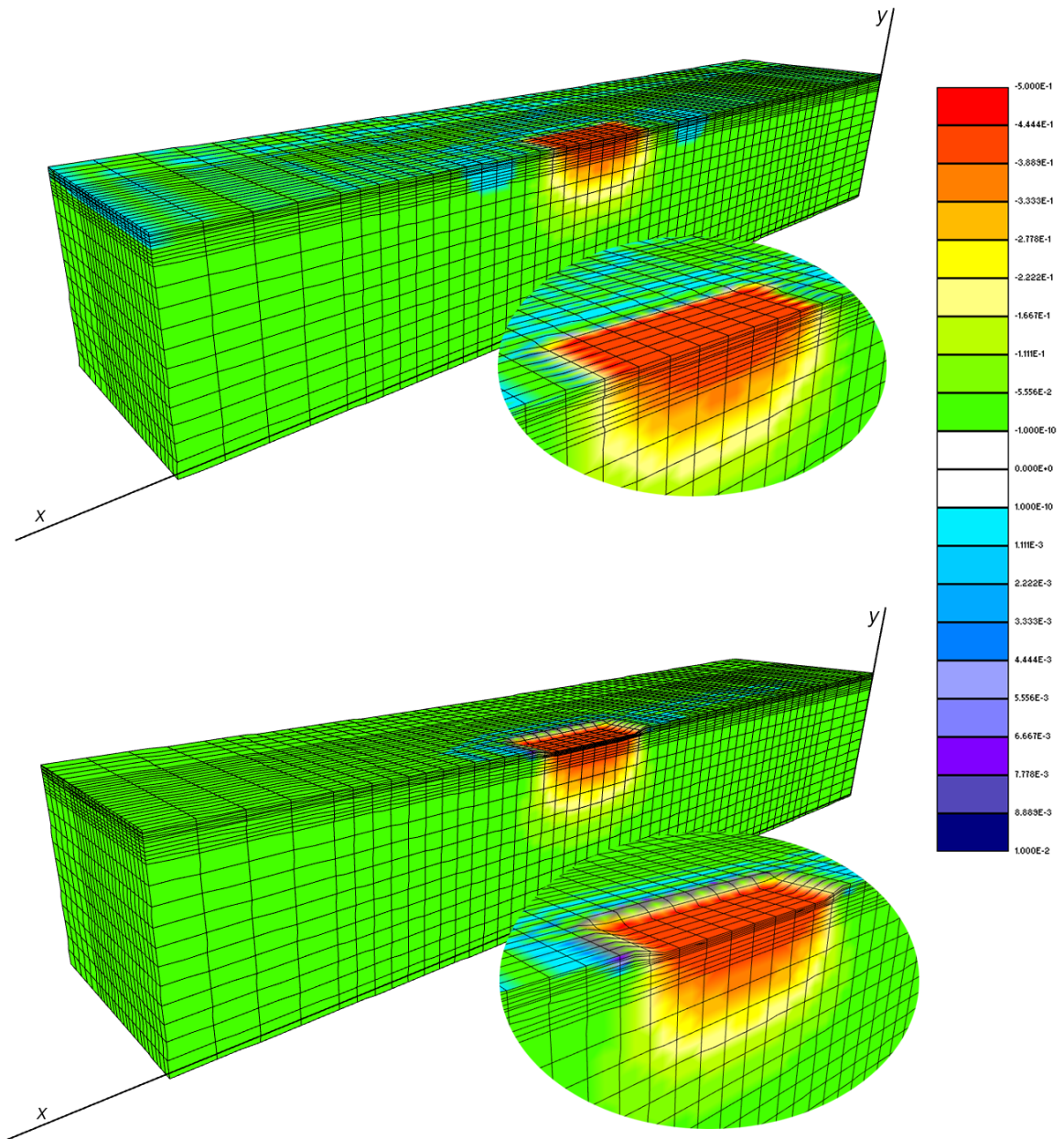


Figure 8.3: Enhanced displacement under the load and stresses ( $\sigma_{yy}$ ) for Mixture A (top) and Mixture C (bottom)

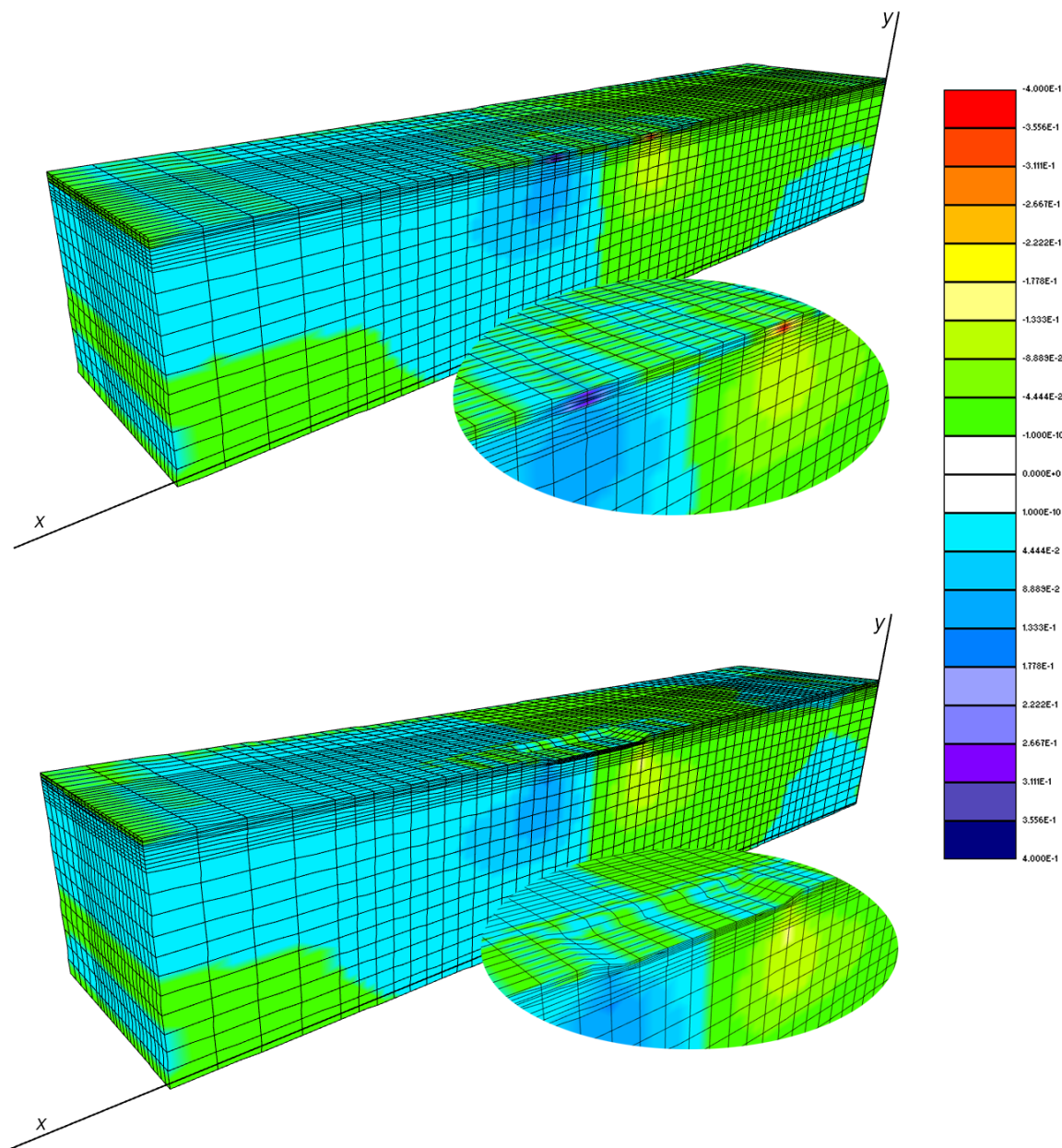


Figure 8.4: Enhanced displacement under the load and shear forces ( $\tau_{xy}$ ) for Mixture A (top) and Mixture C (bottom)

From the figure 8.2, we see that the stiffness of the top layer has a great influence on the stress distribution through the entire road section. Where for Mixture A, the stresses are mainly absorbed by the top USP layer, for Mixture C these stresses are more distributed over the underlying materials.

For the vertical stresses  $\sigma_{yy}$ , this effect is smaller. Here, hardly any difference is seen between the 2 models shown in figure 8.3. The elasticity of Mixture C, however, allowed some wave-forming in front of the load, where tensile stresses occur.

For the shear stresses, shown in figure 8.4, again a difference is observed. The stiffer Mixture A carries almost all shear forces, but with the more elastic Mixture C, those shear forces are more spread over the complete system.

## 8.5. Conclusion

The difference in stiffness for the USP layer has a large effect on the occurring stresses in both the USP and the underlying layers of the road construction. By choosing a more elastic top surface layer, the stresses in the lower part of the construction become higher than with a stiff surface layer. However, with a stiff top layer, the stresses in this top layer increase. For Mixture A, these tensile stresses can go up to 0.5 MPa, which is less than its capacity as shown in chapter 3. In this research, no information is gathered on the effect of fatigue loading, but since 0.5MPa is almost 30% of its capacity after moisture conditioning, more information on this must be gained.

Because of time limitations, this run is performed without the application of an interface layer. Further research on this, by the use of a model with an interface layer between the USP and the porous asphalt, might give more information on the occurring tensile forces in the interface. Based on this, demands for the strength at the tensile adhesion test can be made and investigated in a laboratory environment.

# Conclusion and Recommendations

## 9.1. Conclusion

The literature points out that for various previous field tests, moisture conditioning has a great negative effect on the strength of the new ultra silent pavements. To get more insight in the materials' behaviour, three new materials are tested in a laboratory environment. With the Indirect Tensile Test (ITT) and the moisture conditioning protocol which is applied on the ITT specimens, it is concluded that two of the three new materials, indeed greatly decreases in strength due to moisture conditioning. Also, the application of the cyclic pore pressure proofs to have a great effect on a stiff mixture like Mixture A, for which is shown that the lack of deformation capacity negatively affects the strength of the material.

The ageing protocol does not seem to affect two of the three materials as much as expected. For the third material, it cannot be concluded that its properties changed due to the time in the oven or because of its actual age. Already for the fresh and unaged specimens, a great increase in strength over the 4 weeks of testing is seen and therefore the effect of spending 4 weeks in the oven at 60°C is unclear.

With the stiffness test, the great difference between the 3 tested materials is shown. It shows that all mixtures have a different behaviour when it comes to viscosity. Mixture A increases in stiffness with the increase of the loading frequency, but flattens out in the second half of the master curve. Mixture B has a steep ramp in the master curve in the area where traffic loading frequencies are located and mixture C behaves almost as a fully elastic material. The behaviour of Mixture C is favourable, because of its predictability. Mixture B behaves different for almost every change in temperature or loading frequency, and Mixture A can become very unpredictable at very hot days.

This behaviour can also be concluded from the cohesive strength test: Mixture C has the same values for almost all tests, while Mixture B varies a lot between the various tests. This is because the strain rates and temperatures can put the cohesive test in the area where the master curve of Mixture B is the steepest. For Mixture A, at this point the master curve already flattens out, so not much difference in the results is found.

From the results of Tensile Adhesion Test (TAT) it is clearly visible how much influence the moisture conditioning has on the strength of the interface layer. In all cases, the adhesion strength decreases and in all cases, the adhesion becomes too low. Even in the unconditioned state, only for 1 mixture the interface is strong enough to make the specimen break in the asphalt instead of in the interface. This is partly because of the open structure and the differences in aggregate size of the 2 layers. Already when glueing the porous asphalt to the aluminium cap of the test setup, a lot of glue is needed to fill the pores and extend the contact area.

From the finite element analysis is clear that the mixture composition has great influence on the diffusivity of the mixture. Mixture A, with a very high amount of air voids, saturates very fast and a change in the moisture diffusion coefficient has a large effect. For mixture C, where all aggregates are packed in rubber, the change in saturation speed is much lower, indicating less susceptibility to moisture

damage. However, there are too many unknowns for this model while performing the moisture diffusion analysis to take more specific conclusions from these runs. In order to get more information via this finite element analysis, more input data is needed.

With the moving wheel-load simulation is shown that the stiffness of the top layer influences the distribution of the stresses due to the wheel-load. Especially for the stiff Mixture A, this results in high tensile stresses in the bottom elements of the USP layer. Repetitive loading can result in fatigue failure of the USP, but no further fatigue behaviour information is available for this material. With the elastic Mixture C, the stresses are more distributed over the entire pavement structure. Therefore, this results in higher stresses in the lower layers and interfaces than with Mixture A and can therefore result in failure of the lower asphalt layers. This coincides with the results of the field test in Stockholm, where very elastic types of PERS were tested [6].

In the end we it can be said that with those 2 methods, both the laboratory and the computational method, a lot of knowledge about the influence of moisture on the mechanical properties of Ultra Silent Pavement mixtures can be retrieved. Those methods are more reliable and better controllable than expensive field tests. In the future, it will be easy for manufacturers to change the composition and perform certain tests again, within in a limited period of time.

## 9.2. Recommendations for further research

For future testing, it is not necessary to change a lot regarding the laboratory tests. The main problem here is the fact that none of the mixtures were known when the tests to perform had to be determined, which resulted in one mixture not being suitable for the indirect tensile test. However, even in this case, it is fairly simple to switch to the direct tensile test and still compare the results in a fair way. However, more research can be done on fast hardening adhesives which might be used to glue the samples in the test setups. During this research, the only glue available being strong enough, needs 24 hours to dry, which cost a lot of time in preparation.

On the computational part of this research, a lot of improvement can be be made. For the moisture diffusion models, the results will be much more reliable when the moisture diffusion coefficients of the different used materials are known.

For the moving wheel load, the model might be fitted with an interface layer to get more reliable information about the occurring stresses in this interface. These stresses can then be compared with the strengths of the interface as determined via the tensile adhesion test. Also, the patch load that is used in this research can be replaced with a load patch that is more equal to a real wheel load patch. Furthermore, different scenario's with respect to load cases, moving speeds, forces etc. need to be investigated.

# Bibliography

- [1] J. I. Halonen, *European Heart Journal*, 2015.
- [2] U. Sandberg et al., *Poroelastic Road Surface (PERS): A review of 30 years of R&D work*, 2011.
- [3] T. Zetterling, N. Nilsson, *Implementation of the Poroelastic Road Surface*, 1990.
- [4] U. Sandberg, J. Ejsmont, *Tyre/Road reference book*, 2002.
- [5] M. Liu, X. Huang, G. Xue, *International Journal of Sustainable Built Environment*, 2016.
- [6] U. Sandberg, B. Kalman, *The Poroelastic Road Surface – Results of an Experiment in Stockholm*, 2005.
- [7] H. Fujita, Y. Arao, K. Hamada, *Performance of the Porous Elastic Road Surface (PERS) as LowNoise Pavement*, 2011.
- [8] K. Kubo, *Present Status of Porous Elastic Rubber Surface (PERS) in Japan*, 2011.
- [9] R. Hofman, P. The, W. van Vliet, *Results Dutch PERS test on A50*, 2011.
- [10] L. Goubert, U. Sandberg, *The PERSUADE project: developing the concept of poroelastic road surface into a powerful tool for abating traffic noise*, 2010.
- [11] P. Kandhal, C. Lubold, F. Roberts Jr., *Water damage to asphalt overlays: Case histories*, 1989.
- [12] A. Varveri, S. Avgerinopoulos, A. Scarpas, A. Collop, S. Erkens, *On the combined effect of moisture diffusion and cyclic pore pressure generation in asphalt concrete.*, 2014.
- [13] A. Varveri, S. Avgerinopoulos, A. Scarpas, *Experimental Evaluation of Long and Short Term Moisture Damage Characteristics of Asphalt Mixtures*, 2014.
- [14] A. Varveri et al., *Influence of Air Void Content on Moisture Damage Susceptibility of Asphalt Mixtures - Computational Study*, 2014.
- [15] B. Hollingsworth, K. Ledbury, A. Stokoe, *The accelerated ageing of some commercial polyurethane rubbers*, 1967.
- [16] G. Odegard, A. Bandyopadhyay, *Physical Aging of Epoxy Polymers and Their Composites*, 2011.
- [17] T. Chang, J. Brittain, *Polymer Engineering and Science*, 1982.
- [18] C. Raab, M. Partl, *Interlayer shear performance: experience with different pavement structures*, 2004.
- [19] S. Srirangam, K. Anupam, A. Scarpas, C. Kasbergen, *A Durability Analysis of Super-Quiet Pavement Structures by Finite Element Method*, 2015.
- [20] E. C. for Standardisation (CEN), *NEN-EN 12697-23: Bituminous mixtures - Test methods for hot mix asphalt - Part 23: Determination of the indirect tensile strength of bituminous specimens*, 2004.
- [21] F. Pramesti, *Laboratory and Field Asphalt Fatigue Performance*, 2015.
- [22] S. M. J. G. Erkens, *Asphalt Concrete Response (ACRe) - Determination, Modelling and Prediction*, 2002.
- [23] E. C. for Standardisation (CEN), *NEN-EN 12697-46: Bituminous mixtures - Test methods for hot mix asphalt - Part 46: Low temperature cracking and properties by uniaxial tension tests*, 2012.

- [24] E. C. for Standardisation (CEN), *NEN-EN 12697-26: Bituminous mixtures - Test methods for hot mix asphalt - Part 26: Stiffness*, 2003.
- [25] K. P. Biligiri et al, *Understanding the fundamental material properties of low-noise poroelastic road surfaces*, 2011.
- [26] M. R. Poot, *CT 4880 - Asphalt Testing (manual)*, 2014.
- [27] T. O. Medani et al, *Constructing the Stiffness Master Curves for Asphaltic Mixes*, 2003.
- [28] C. Raab, M. Partl, *Interlayer shear performance: Experience with different pavement structures*, 2004.
- [29] F. Rezaei, F. Sharif, A. A. Sarabi, S. M. Kasiriha, M. Rahmanian, E. Akbarinezhad, *Evaluating water transport through high solid polyurethane coating using the EIS method*, 2010.
- [30] S. Dutaa, *Water absorption and dielectric properties of Epoxy insulation*, 2008.
- [31] E. Arambula, S. Caro, E. A. Masad, *Experimental measurement and numerical simulation of water vapor diffusion through asphalt pavement materials.*, 2010.
- [32] E. Kassem, E. Masad, R. Lytton, R. Bulut, *Measurements of the moisture diffusion coefficient of asphalt mixtures and its relationship to mixture composition.*, 2009.